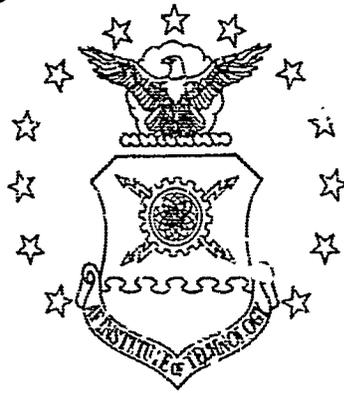AD NUMBER

AD860077

NEW LIMITATION CHANGE

TO

Approved for public release, distribution unlimited

FROM

Distribution authorized to U.S. Gov't. agencies and their contractors; Critical Technology; DEC 1968. Other requests shall be referred to Air Force Institute of Technology, Dean of Engineering, Attn: AFIT-SE, Wright-Patterson AFB, OH 45433.

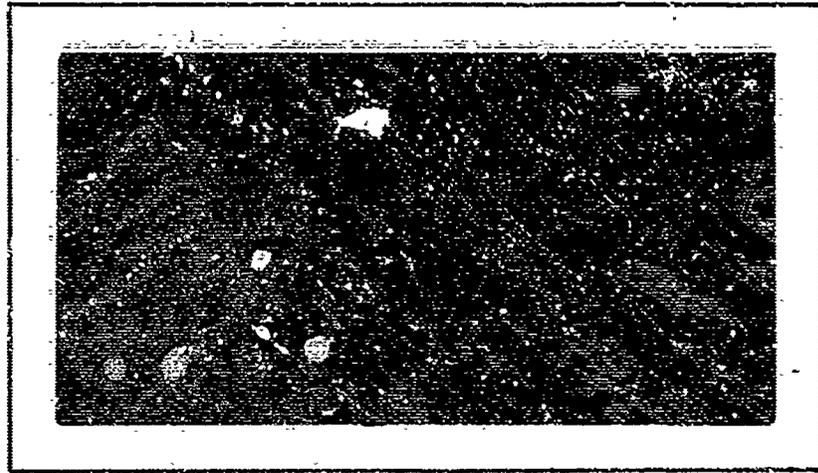AUTHORITY

AFIT Memo dtd 22 Jul 1971

AIR FORCE INSTITUTE OF TECHNOLOGY

AIR UNIVERSITY
UNITED STATES AIR FORCE

SCHOOL OF ENGINEERING

WRIGHT-PATTERSON AIR FORCE BASE, OHIO

SOME PARAMETER INFLUENCE ON THE FAILURE

MODE OF SIDE - ON AIR BLAST LOADED CYLINDERS

THESIS

GAW/MC/68-13

Richard C. Pees
2/Lt   USAF

AFLC-WFAFB-SEP 69 30

SHELL PARAMETER INFLUENCE

ON THE

FAILURE MODE OF SIDE - ON AIR BLAST LOADED CYLINDERS

THESIS

Presented to the Faculty of the School of Engineering of

the Air Force Institute of Technology

Air University

in Partial Fullfillment of the

Requirements for the Degree of

Master of Science

by

Richard Conrad Pees

2/Lt   USAF

Graduate Air Weapons

December 1968

Preface

I would like to express my special thanks to Dr. W. Schuman for suggesting this thesis topic. In addition to this initial help, he provided supplemental support by testing shells of special interest to this study.

I would like to express my thanks to Dr. D. Norris for his special help in the analysis of non-linear differential equations and the resulting solutions thereof.

During the final preparation of this paper, many drastic problems came to light. As a result, extra hours and days of consultation had to be spent with my thesis advisor, Major W. Goldberg. I wish to acknowledge my indebtedness to him for his invaluable assistance and his time.

I also wish to acknowledge my indebtedness to my wife for her understanding and assistance in the preparation of this report.

RICHARD C. PEES

List of Symbols

$\epsilon_x, \epsilon_\theta, \gamma_{x\theta}$	strain components
ν	Poisson's ratio
E	Young's modulus, psi
E_t	Tangent modulus, psi
σ_y	tension yield stress, psi
ϵ_y	yield strain
D_f	flexural rigidity, $Eh^3 / 12(1 - \nu^2)$
ρ	mass density per unit volume
ζ	mass density per unit length
a	radius, in
D	diameter, in
h	thickness, in
L	length, in
t	time, msec
ζ	thickness parameter, $h^2 / 12\, a^2$
P	pressure, psi
P_r	reflected pressure, psi
U, V, W	displacements in x, θ, z directions
u, v, w	non-dimensional U, V, W
κ, ι, μ	virtual displacements in x, θ, z directions
η	centerline curvature
$\eta_x, \eta_{x\theta}, \eta_\theta$	curvature change components
Q	shear force load
$N_x, N_\theta, N_{x\theta}$	force components
M	moment

$M_x, M_\theta, M_{x\theta}$	moment components
I_r	reflected impulse, psi – msec
ξ	non-dimensional variable, x/a
λ	non-dimensional variable, $\Box/a$
τ	non-dimensional time, ct/a
ψ	non-dimensional pressure parameter, $p_1 / p_c + p_1$
I	moment of inertia
q_n, ω_n	non-dimensional frequencies
p_o'	non-dimensional pressure
Δ	constant
β	constant, $1.5 \, a^4 \, (1 - \nu^2) / h^2$
η	constant, $a^5 \, (1 - \nu^2) / h^2$
V_e	potential energy
U_m	membrane strain energy
V_b	bending strain energy
Ω	potential energy of external forces
A_{ij}	constant coefficients
$A_n(t)$	time varying coefficient
$\overline{F}$	external force vector
Γ	decay parameter (/msec), p_r / I_r
$F_w, F_b, F_t, F_{\omega o}$	non-dimensional scale factors

List of Figures

v

List of Tables

Abstract

The purpose of this investigation is to determine the influence of the shell size parameters, length-to-diameter ratio and diameter-to-thickness ratio, on the failure modes of cylinders under side-on air blast loading. These failure modes are: 1) hinge collapse, 2) wave buckling, and 3) combination. The results of this study show that the diameter-to-thickness, (D/h), ratio dominates the shell behavior and that for values of D/h below 110, hinge collapse seems to be dominant; between 110 and 450, combination failure seems to be dominant; above 450, wave buckling seems to be dominant. In addition, the dynamic buckling theory seems to predict hinge collapse and combination failures when the D/h ratio is below 300.

Contents

SHELL PARAMETER INFLUENCE

ON THE

FAILURE MODE OF SIDE - ON AIR BLAST LOADED CYLINDERS

I. Introduction

The failure of aerospace structures subjected to side-on air blast
loading has received intensive investigation by several different groups
in the last few years. The results of these intensive investigations
indicate that the main structures of aerospace vehicles (cylinders)
fail in one of three modes. These mode shapes are hinge collapse, wave
buckling, and combination patterns. The hinge collapse mode is charac-
terized by the formation of a plastic hinge line perpendicular to the
longitudinal axis of the cylinder. The wave buckling mode is character-
ized by the formation of ripple waves in the circumferential direction
and one-half wave in the longitudinal direction. The combination pat-
tern is characterized by the simultaneous presence of the previously
mentioned modes.

The time history of the actual formation of the failure pattern of
these aerospace structures has not been determined, rather a criterion
has been established that specifies if a structure will fail. This
criterion states that when the pressure and impulse generated by the
blast reach the proper magnitudes at the position of the structure,
the structure will fail. Those magnitudes of pressure and impulse which
produce failure are called critical pressure and critical impulse. The
tabulation of these values is dependent upon the structure material,
type of explosive, and structure position from the point of detonation.
Once having such a set of values, the construction of iso-damage curves

1

is possible. These iso-damage curves are the result of a graphical representation, on a logarithmic scale, of the critical values of pressure and impulse. The shape of these curves resemble hyperbolas and define the boundary between failure and non-failure of a given structure.

The one disadvantage of the above mentioned curves, is that they (curves) do not predict how a structure will fail, or what is the dominant shell parameter in determining the type of failure mode.

The first section of this paper deals with background material. The second section defines the problem, lists the assumptions, and gives the scope and method of approach. The third section developes the theory used in discussing the various failure modes. The next section discusses the effect of the shell parameters in determining the failure mode and the last section presents the conclusions.

II. Background

One of the major problems in the design of structures is that of determining their useful life. In determining the useful life span of a structure it is necessary to define the failure modes of the structure and the reasons for failure. This needs to be done so that design judgements can be made as to how to reinforce a particular shell geometry to prevent its failure.

In extensive experimentation conducted by Schuman, at Ballistic Research Laboratories, Maryland (Ref 13), the conclusion was reached that when an aerospace vehicle is subjected to side-on blast loading of sufficient magnitude to cause incipient failure, it will fail in one of three ways - hinge collapse, wave buckling, or a combination pattern. Since most aerospace vehicles are primarily of cylindrical shape, Schuman used as his model cylindrical shells with rigidly clamped ends. He surmised that the clamped ends would closely approximate the bulkheads found between actual sections of an aerospace vehicle. As a result of clamping the ends, he assumed that no pre-loads such as bending, compression or torsion were present. In order to construct iso-damage curves, Shuman chose as his failure criterion a permanent radial deflection of 10% of the original diameter. After determining if the shell met the failure criterion, he used a set of curves given in Reference 9 to obtain the critical values of pressure and impulse. These values were then compared to the values obtained from instrumented shells and the agreement was found to be within the experimental error. Having constructed the iso-damage curves, Schuman was then able to predict at what combination of pressure and impulse a shell of given dimension and material would be expected to fail. The curves constructed were only

for three types of aluminum and one mild steel. These iso-damage curves made no attempt to predict the type of shell failure mode.

J. E. Greenspon of J. G. Engineering Research Associates (Ref 10), used an energy approach to calculate the energy necessary for a given deflection shape to occur. He used elastic stress analysis, membrane theory, and Von Mises yeild condition to determine an expression for the critical collapse blast pressure and a formula derived by Timoshenko (Ref 14) for critical buckling blast pressure. By using the smaller of these two values, Greenspon was able to predict whether the shell collapsed or buckled under side-on air blast loading. Once the failure mode was determined, he proceded with a plastic analysis to calculate the energy of deformation. Then assuming that the energy of deformation equals the initial kinetic energy of the shell due to the blast loading, which is related to the applied impulse, he was able to determine the critical impulse required for shell failure. Relating this impulse to critical pressure through relationships developed by H. J. Goodman (Ref 9), Greenspon was able to construct a set of iso-damage curves for collapse and buckling. However these curves still did not determine the role that each shell parameter played in determining the failure mode.

D. L. Anderson and H. E. Lindberg, Stanford Research Institute (Ref 2), developed a dynamic buckling theory for pulse loaded cylindrical shells. In their development they used three mathematical models to describe shell response to pressures varying from ideal impulsive loading to step fuction loading. They chose the tangent modulus model for impulsive loadings which produced plastic flow buckling. They chose the strain reversal model for intermediate duration loadings, which produced plastic-elastic buckling. They chose the elastic model for step pulse loadings, which produced elastic buckling. Using these models in

connection with experimental data, they were able to determine the
equations for the families of .so-damage curves. The resultant equations
were sensitive to variations in geometry, Young's modulus, and shell
density. The end conditions on their shells were assumed to be simply
supported and infinite in length. Their reasoning will be discussed on
page 11.

John P. Anderson and James H. Woodward at Kaman Nuclear, Colorado
Springs, Colorado (Ref 3), approached the case of dynamic hinge collapse,
due to realistic blast pressures, using an energy analysis and the
assumptions of finite length and non-symmetric side-on air blast load-
ing. The particular energy method used was the principle of minimum
potential energy. The pressure distribution that they used was an
exponentially decaying cosine distribution. The equations resulting
from this approach are then solved for a simply supported cylinder using
a Fourier Sine series which has time varying coefficients as the assumed
deflection shape. This deflection shape corresponds to a simply supported
shell. A collapse failure was assumed to occur whenever the maximum
moment, calculated from the deflection shape, equaled or exceeded
Brazier's collapse moment (Ref 6:109).

In a later work by Anderson and Woodward (Ref 4), a static hinge
collapse theory was developed. This theory made use of existing shell
theory and the assumptions that the cylinder is elastic, isotropic, and
infinite in length. The final form of their equations was derived by
assuming that 1) the deflection shape could be represented by a Fourier
Sine series with unknown coefficients, 2) the beam bending mode was
responsible for the primary response of the shell, 3) the breathing and
ovalization modes are secondary, and 4) the shell is inextensional in
the circumferential direction. This last assumption made it necessary

to modify the equilibrium equations to remove their sensitivity to this condition.

In spite of the fact that all of these researchers have investigated the same general problem, namely the response of thin walled cylindrical shells to transverse pressures, no results are presently available which can tell the engineer the answer to two basic questions. First, which shell parameters play the most important role in defining the iso-damage curve of a given shell. Second, what mode of failure will result from application of a given pressure and impulse.

III. Problem

Problem Statement

The problem is to determine how the shell parameters influence the failure modes of right circular cylinders, with clamped ends, due to side-on air blast loading.

The shell parameters are length to diameter ratio (L/D), diameter to thickness ratio (D/h), density (ρ), and modulus of elasticity (E).

Scope

The pressures mentioned in this paper are all reflected pressures as opposed to incident pressures.

The blast loading on the shells are cosine squared and exponential decay cosine distributions. These loadings are on the lateral surface facing the explosive charge. Thus only side-on loading is considered.

The coordinate system that will be used and the failure patterns that will be discussed are illustrated in figures (1) and (2).

The shells of interest are those with L/D ratios of 1 to 5 and D/h ratios of 100 to 700. These shells have been subjected to pressures and impulses that range from impulsive loading to step function loading. The end conditions of the shells are considered to be clamped. The shells are made of 1040 steel, 6061-T6, 5052-H38, and 1100-0 aluminum and are void of internal or external reinforcements.

Assumptions

In addition to the assumptions made by the researchers listed in the background section, the following assumptions are made.

1. The shells are void of any pre-stresses.

2. The relationship between the moment and center line curvature is valid for every cross section.

3. The body forces are zero.

4. The breathing mode is neglected and is independent of collapse mode.

5. The deflection in the longitudinal and tangential directions are small compared to the deflections in the radial direction.

Method of Approach

1. Develope the necessary theory to predict the critical values of pressure and impulse.

2. Plot several iso-damage curves and analyze the general effect of L/D and D/h ratios on the particular failure obtained. By this analysis the most important parameter can be determined.

3. From the equations developed in step (1), solve for a pressure parameter, $p_r \times 10^6 / \varepsilon$, and graph this parameter vs the most important shell ratio while holding the other ratio constant. By plotting this pressure parameter for each theory – dynamic and static buckling and collapse – the upper and lower bounds for each type of failure mode can hopefully be obtained.

This method depends on the developed theory for the dynamic collapse case and the solution of the subsequent expression for the critical pressure. The necessary theory for the cases of dynamic and static buckling and static collapse have essentially been developed and solved by previous researchers.
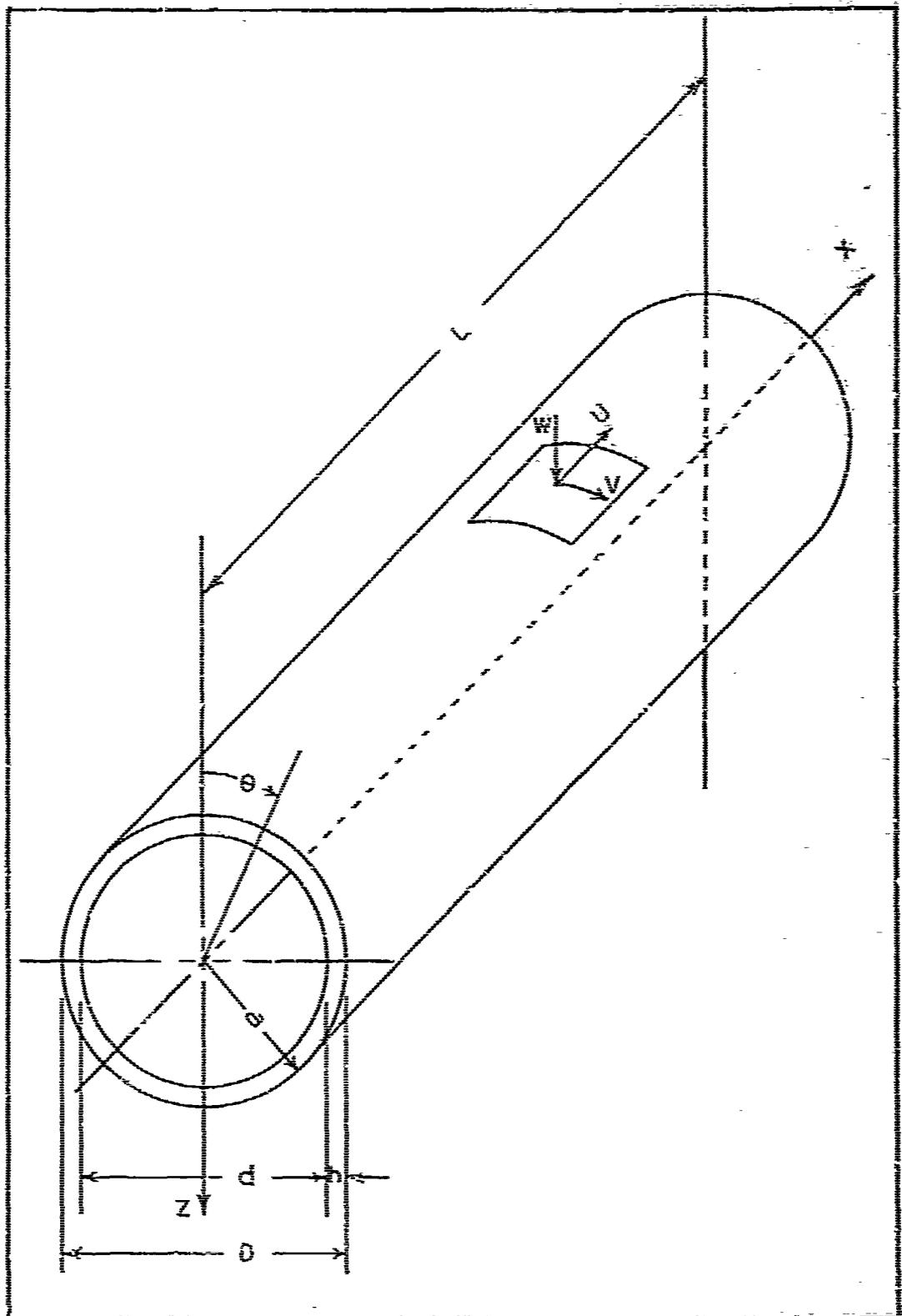
FIGURE I

COORDINATE SYSTEM

9

HINGE COLLAPSE PATTERN

WAVE BUCKLING PATTERN
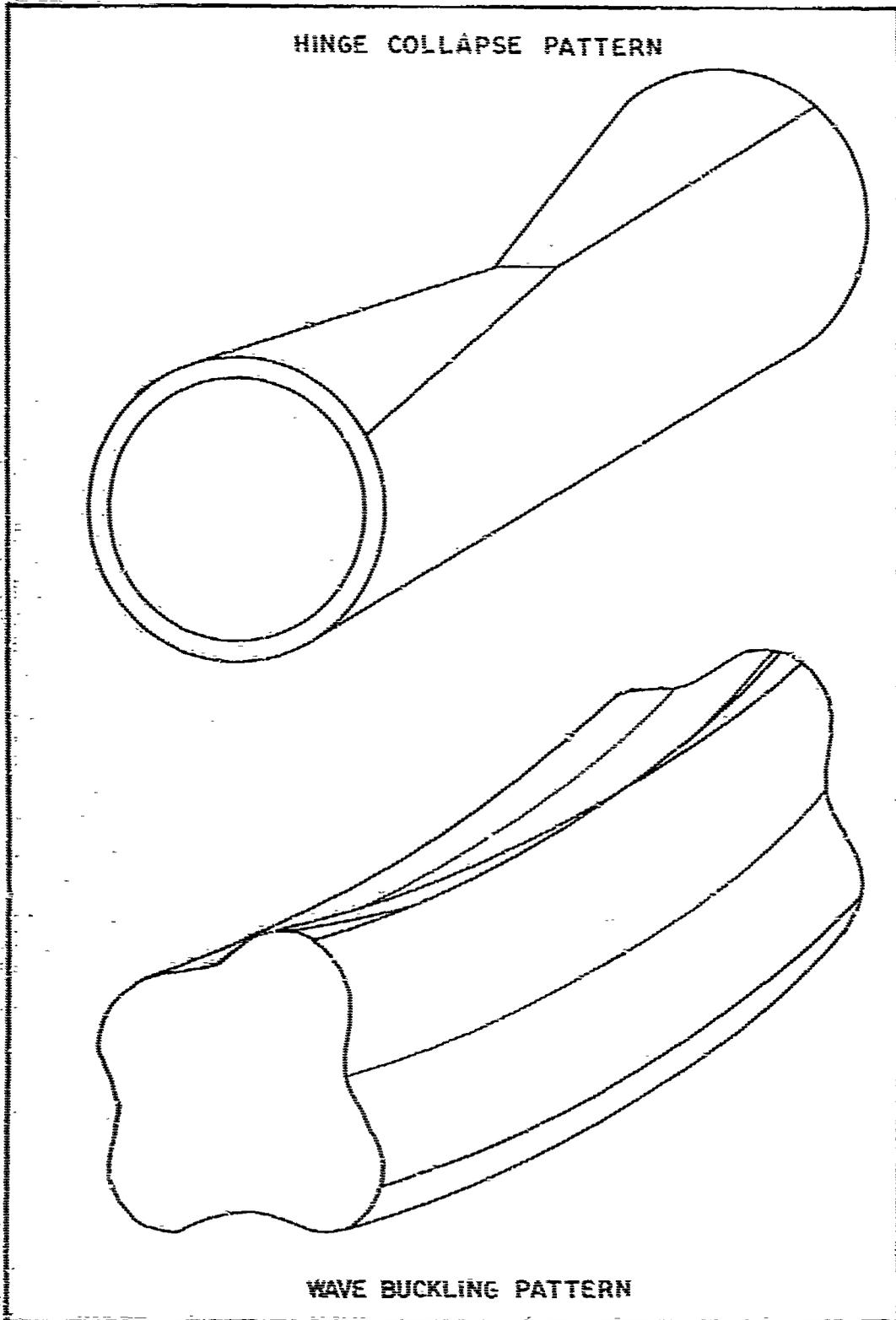
FIGURE 2

IV. Theory

Dynamic Buckling Theory

In treating the case of dynamic wave buckling, three models are used to describe the failure mode. Each model predicts shell behavior in one of the three realms of pressure loading - impulsive, quasi-impulsive, and quasi-static. The primary characteristic of each realm is impulse, impulse and pressure, and peak pressure respectively. In the theory development which follows, the tangent-modulus model is used for impulse loads, the strain-reversal model for quasi-impulsive loads, and the elastic model for quasi-static loads.

Tangent-Modulus Model. The deformation in this region takes place during membrane plastic flow, without strain reversal, and is governed by the tangent modulus (Ref 2:198). Since the shell response is of relatively high order modes, the effects of the ends are unimportant beyond a few wavelengths from the end; thus the shell can be treated as infinitely long (Ref 2:198).

Assuming an itital shell deflection of zero, an inward radial deflection as positive, and the displacement during shell motion as $W(\theta,t)$, the curvature change of the shell is given by (Ref 2:201)

$$\eta(\theta,t) = \frac{1}{a^2}\left(\frac{\partial^2 W}{\partial \theta^2} + W\right) \tag{1}$$

where a is the shell radius. The curvature can also be expressed as rotation per unit arc length (Ref 2:201), and is given by

$$\frac{1}{a}\frac{\partial \bar{\phi}}{\partial \theta} = \frac{1}{a} + \eta \tag{2}$$

where $\partial \bar{\phi}$ is the angle defined in Figure 3. Using the above relations,

11

the dynamic equilibrium equation in the radial direction per unit axial length, becomes

$$- \frac{1}{a} \frac{\partial Q}{\partial \theta} - \frac{N_\theta}{a} \frac{\partial \widehat{\phi}}{\partial \theta} + p - \rho h \frac{\partial^2 W}{\partial t^2} = 0 \qquad (3)$$

where $N_\theta(\theta,t)$ is the membrane force, $Q(\theta,t)$ is the shear force per unit length, and $p(\theta,t)$ is the side-on pressure, positive as shown in Figure 3. By neglecting rotary inertia and summing moments on the element shown in Figure 3.

$$Q = \frac{1}{a} \frac{\partial M}{\partial \theta} \qquad (4)$$

But

$$M = M(\theta,t) = \frac{E_t I \eta}{1 - \nu^2} \qquad (5)$$

where E_t is the tangent modulus, I is the moment of inertia of the shell, and ν is Poisson's ratio. Defining

$$a^2 = \frac{h^2}{12 a^2} \qquad (6)$$

$$c^2 = \frac{E}{\rho} \qquad (7)$$

$$\omega = \frac{W}{a} \qquad (8)$$

$$\tau = \frac{ct}{a} \qquad (9)$$

$$\sigma_\theta = \frac{N_\theta}{h} \qquad (10)$$

$$p'(\theta,\tau) = p(\theta,t) \frac{a(1 - \nu^2)}{Eh} \qquad (11)$$
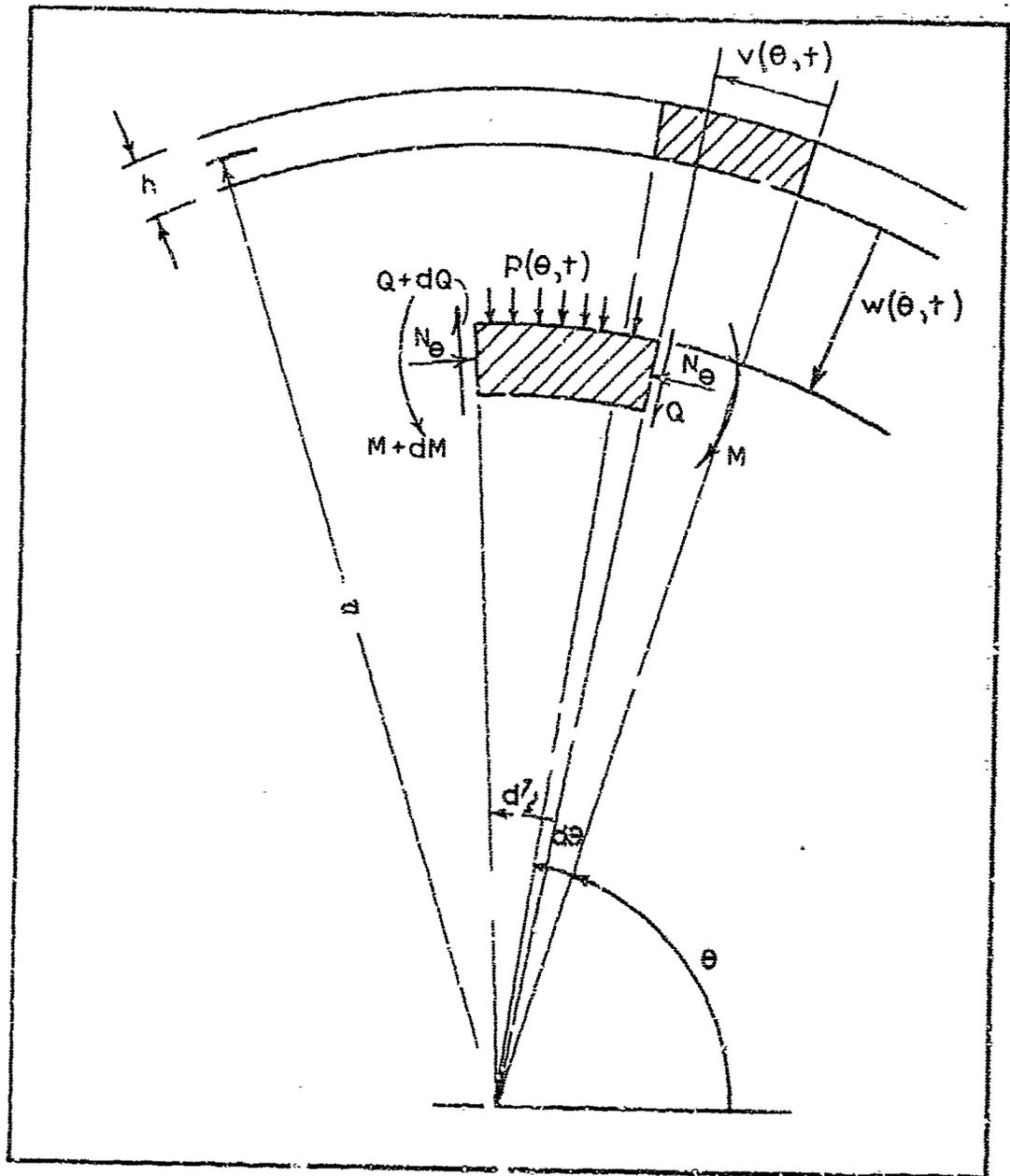
FIGURE 3

FORCES ON SHELL ELEMENT
Ref (2:20)

Substituting equations (2), (4) to (11) by use of equation (1) into equation (3) yields

$$\frac{\partial^2 \omega}{\partial T^2} + \frac{a^2 E_t}{E}\frac{\partial^2 \omega}{\partial \theta^2} + \left[\frac{a^2 E_t}{E} + \frac{\sigma_\theta(1-\nu^2)}{E}\right]\frac{\partial^2 \omega}{\partial \theta^2}$$

$$+ \frac{\sigma_\theta(1-\nu^2)}{E}(1+\omega) = p' \tag{12}$$

Since the shell is assumed inextensional, the effects of the flexural modes on the average circumferential strain is restricted to second order terms (Ref 8:269). The assumed radial deformation and pressure distribution are given by

$$\omega(\theta,T) = \omega_0(T) + \sum_{n=1}^{\infty} \omega_n(T)\cos n\theta \tag{13}$$

$$p'(\theta,T) = p'_0(T) + \sum_{n=1}^{\infty} p'_n(T)\cos n\theta \tag{14}$$

Substituting these relationships into equation (12), equating coefficients, and assuming $W_0(T)$ is negligible compared to unity (Ref 2:205) the resulting equations of motion are

$$\frac{\partial^2 \omega_0}{\partial T^2} + \frac{\sigma_\theta(1-\nu^2)}{E} = p'_0 \tag{15}$$

$$\frac{\partial^2 \omega_n}{\partial T^2} + (n^2-1)\left[\frac{n^2 a^2 E_t}{E} - \frac{\sigma_\theta(1-\nu^2)}{E}\right]\omega_n = p'_n \tag{16}$$

$$n = 1,2,3\cdots$$

14

For impulsive loads, the pressure terms in equations (15) and (16) vanish. The initial conditions are

$$u_n(0) = 0 \tag{17}$$

$$\frac{\partial u_n(0)}{\partial T} = \frac{I_n}{\rho h c} \qquad n = 0,1,2,3\cdots \tag{18}$$

where

$$I(\theta) = I_o + \sum_{n=1}^{\infty} I_n \cos(n\theta) \tag{19}$$

is the impulse applied to the shell.

Equation (15), which governs the motion of the radial mode, is solved in two parts, depending upon the value of σ_θ. If we take σ_y and ϵ_y as the yield stress and yield strain and E_o a the stress-strain modulus beyond the yield point, then

$$\sigma_\theta = \frac{E}{1-\nu^2} w_o \quad, \qquad 0 \le w_o \le (1-\nu^2)\epsilon_y \tag{20}$$

$$\sigma_\theta = \sigma_y + \frac{E_o}{1-\nu^2}\left[w_o - (1-\nu^2)\epsilon_y \right] , \quad (1-\nu^2)\epsilon_y < w_o \tag{21}$$

Thus equation (15) becomes

$$\frac{\partial^2 w_o}{\partial T^2} + w_o = P_o \quad , \qquad 0 \le w_o \le (1-\nu^2) \tag{22}$$

$$\frac{\partial^2 w_o}{\partial T^2} + \frac{E_o}{E} w_o = -\left(1 - \frac{E_o}{E} \right)(1-\nu^2)\epsilon_y + P_o \quad , \quad (1-\nu^2)\epsilon_y < w_o \tag{23}$$

which can readily be solved.

Equation (16), which governs the motion of the flexural modes, is solved by assuming σ_θ and E_t constant (Ref 2:206). Applying condition (17) and (18) to equation (16) the solution is

15

$$u_n(\tau) = \frac{\partial u_n(\tau_y)}{\partial \tau} \frac{\text{SINH } q_n(\tau - \tau_y)}{q_n} \tag{24}$$

where τ_y is the time at which yielding first occurs and

$$q_n^2 = (n^2 - 1)\left[\frac{\sigma_\theta(1 - \nu^2)}{E_t} - n^2 a^2\right] \frac{E_t}{E} \tag{25}$$

The most amplified flexural mode, n, occurs at the maximum value of q_n which gives n as the integer nearest to (Ref 2:214)

$$n = \sqrt{\frac{1}{2}\left(\frac{\sigma_\theta(1 - \nu^2)}{a^2 E_t}\right)} = \frac{a}{h}\sqrt{\frac{6\sigma_\theta(1 - \nu^2)}{E_t}} \tag{26}$$

Equation (26) shows that the most amplified flexural mode is directly dependent on a/h and $\sqrt{\sigma_\theta/E_t}$. From equation (25), the ratio σ_θ/E_t determines the sign of q_n^2 thus determining whether the motion is hyperbolic or oscillatory. Hence σ_θ/E_t is the material property that sets the magnitude and type of motion for a shell under impulsive loading (Ref 2:215).

Elastic Model. The deformation of shells in this region is charac terized by long duration pressures and buckle such that their response can be assumed as elastic. Since the buckling behavior is elastic, a reasonable extension of static theory is made by the inclusion of iner- tia terms (Ref 2:198). To determine the membrane force, the end effects are neglected, but it is required that the flexural mode satisfy the boundary conditions (Ref 2:198).

The governing equation of motion is Donnell's equations (Ref 5) with the addition of inertia terms. Thus the equation of equilibrim in the radial direction is

$$D_f \nabla^4 W + N_x \frac{\partial^2 W}{\partial x^2} + \frac{2N_{x\theta}}{a} \frac{\partial^2 W}{\partial x \partial \theta} + \frac{N_\theta}{a^2} \frac{\partial^2 W}{\partial^2 \theta} +$$

$$\frac{N_\theta}{a} + \rho h \frac{\partial^2 W}{\partial t^2} - p = 0 \qquad (27)$$

where N_x, $N_{x\theta}$, N_θ are the membrane forces positive in compression, and

$$D_f = \frac{E h^3}{12(1 - \nu^2)} \qquad (28)$$

is the flexural rigidity of the shell, N_θ can be expressed as (2:207)

$$N_\theta = \frac{E h}{(1 - \nu^2)} \frac{W_o}{a} + \frac{\partial^2 F}{\partial x^2} \qquad (29)$$

where F is the stress function for the membrane forces due to the flexural motion and W_o is the uniform radial deformation. The membrane forces N_x and $N_{x\theta}$ can now be represented as (Ref 2:208)

$$N_x = \frac{\partial^2 F}{a^2 \partial \theta^2} \qquad (30)$$

$$N_{x\theta} = -\frac{\partial^2 F}{a \partial x \partial \theta} \qquad (31)$$

Utilizing the compatibility condition

$$\nabla^4 F = \frac{E h}{a} \frac{\partial^2 W}{\partial x^2} \qquad (32)$$

introducing the non-dimensional variables

$$\xi = \frac{x}{a} \qquad (33)$$

$$\omega = \frac{W}{a} \qquad (34)$$

$$1 = \frac{L}{a} \qquad (35)$$

17

$$T = \frac{ct}{a} \tag{36}$$

and expressing w and p in series form

$$w(\xi,\theta,X) = w_o(T) + \sum_{n=1}^{\infty} w_n(T) \cos n\theta \sin \frac{\pi \xi}{\lambda} \tag{37}$$

$$p'(\xi,\theta,X) = \frac{Eh}{(1-\nu^2)a}\left[p'_o(T) + \sum_{n=1}^{\infty} p'_n(T)\cos n\theta \sin \frac{\pi \xi}{1}\right] \tag{38}$$

equation (32) can be represented as

$$\frac{1}{a^2}\left(\frac{\partial^2}{\partial \xi^2} + \frac{\partial^2}{\partial \theta^2}\right)^2 F = -\frac{Eh}{a^2}\sum_{n=1}^{\infty}\left(\frac{\pi}{1}\right)^2 w_n \cos n\theta \sin \frac{\pi \xi}{1} \tag{39}$$

Thus

$$F = \sum_{n=1}^{\infty} P_n w_n \cos n\theta \sin \frac{\pi \xi}{1} \tag{40}$$

where P_n are constants. This expression for F assumes simple supports and that there exists only one half-wave buckle in the axial direction. These assumptions are based on experimental results of dynamic loadings (Ref 2:208-9).

Using equations (29) to (31), (33) (38), and (40), the equations of motion can be separated into

$$\frac{\partial^2 w_o}{\partial T^2} + w_o = p'_o \tag{41}$$

$$\frac{\partial^2 w_n}{\partial T^2} + \left[\alpha^2\left(n^2 + \frac{\pi^2}{1^2}\right)^2 + \frac{(1-\nu^2)\left(\frac{\pi}{1}\right)^4}{\left(n^2 + \frac{\pi^2}{1^2}\right)^2} - n^2 w_o\right]w_n = p'_n \tag{42}$$

$$n=1,2,3\cdots$$

18

with initial conditions as

$$\omega_n(0) = \frac{\partial \omega_n(0)}{\partial T} = 0 \quad , \quad n = 1, 2, \cdots \qquad (43)$$

. Solving equation (41) for the static case and substitution of the results into equation (42) yields

$$\omega_n = \frac{p_n'}{\left[a^2 \left(n^2 + \frac{\pi^2}{1^2} \right)^2 + \frac{(1-\nu^2)(\pi^4/1^4)}{\left(n^2 + \frac{\pi^2}{1^2} \right)} \right] - n^2 p_o'} \qquad (44)$$

From equation (44) as the denominator approaches zero, $\omega_n \to \infty$ and thus the critical pressure, $(p_o')_{cr}$, is given by

$$(p_o')_{cr} = \frac{1}{n^2} \left[a^2(n^2 + \frac{\pi^2}{1^2}) + \frac{(1-\nu^2)(\pi/1)^4}{(n^2 + \frac{\pi^2}{1^2})^2} \right] \qquad (45)$$

$$n = 1, 2, 3, 4 \cdots$$

(Ref 2:210).

By not assuming the static case for equation (41), the expression for w_0 becomes

$$\omega_o = p_o' + A \sin T + B \cos T \qquad (46)$$

and substituting this expression into equation (42) results in Mathieu type of solutions for w_n (Ref 5:263), and if taken at face value predict instabilities at very low values of coefficients A and B. Instabilities of this type require a constant energy input which, in this case, must come from the kinetic and strain energy of the uniform hoop mode. Numerical integration of equation (42) shows that it requires

19

a large number of oscillations of the hoop mode before the flexural
amplitudes build up to the point where there is sufficient energy trans-
fer to cause permanent deformation (Ref 5:264). Experiments show that
buckling takes place with little or no oscillations and is essentially
a single growth to large deformations, thus the static case which
results in hyperbolic growth is a valid assumption (Ref 2:218). Hence
equation (42) can be rewritten as

$$\frac{\partial^2 w_n}{\partial T^2} + n^2(\omega_n^2 - w_o) w_n = p_n' \tag{47}$$

where

$$(n\omega_n)^2 = a^2\left(n^2 + \frac{\pi^2}{l^2}\right)^2 + \frac{(1-\nu^2)(\pi/l)^4}{\left(n^2 + \frac{\pi^2}{l^2}\right)^2} \tag{48}$$

and the solution is

$$w_n = \frac{\frac{\partial w_n(0)}{\partial T}}{n\sqrt{p_o'-\omega_n^2}} \sinh\left[n\sqrt{p_o'-\omega_n^2}\, T\right] \tag{49}$$

for $p_o' > \omega_n^2$

The most amplified mode of equation (49) corresponds to the maxi-
mum value of $n^2(p_o'-\omega_n^2)$. For $n \gg \frac{\pi}{L}$ and the second term of equation
(48) small compared to the first term, (Ref 2:219), the most amplified
mode is

$$n = \sqrt{p_o'/2a^2} = \sqrt{6p_o(1-\nu^2)/E}\left(\frac{a}{h}\right)^{3/2} \tag{50}$$

Equation (50) shows that the most amplified flexural mode, n, is
directly proportional to $(a/h)^{3/2}$. Thus this ratio seems to dominate
elastic behavior.

Strain Reversal Model. In (Ref 2:236) it is stated:

> "The strain-reversal model to be described in this sec-
> tion predicts threshold buckling loads in the portion of the
> quasi-impulsive load region in which neither the tangent-
> modulus nor the elastic model is applicable. This is done by
> taking into account strains beyond the valid range of the elas-
> tic model and allowing strain reversal and reloading which is
> beyond the valid range of the tangent-modulus model, which
> treats only the initial inward motion of the hoop mode. The
> central conclusion from the solutions using the strain rever-
> sal model is that the curves established by the simpler models
> exhibit the essential characteristics found from the more com-
> plex theory."[a]

The interpretation of the above discussion is that a simple exten-
sion of the tangent-modulus model and the elastic model into the region
governed by the strain reversal model will provide solutions consistent
with experimental results. This is illustrated on Figure 7, page 38 of
this study. Hence no further discussion of this model will be presented
in this study.

Static Buckling Theory

In this buckling analysis, the stability criterion is based upon
the principle of minimum potential energy. The second variation is then
taken and the buckling pressure determined (Ref 1:675). The buckling
pressure is that pressure which will result in the second variation
being positive for a stable state of equilibrium.

The potential energy of the system is given by

$$V_c = U_m + U_b + \Omega \tag{51}$$

where U_m is the membrane strain energy, U_b is the bending strain
energy, and Ω is the potential energy of the external forces. From
(Ref 7:825-830)

$$U_m = \frac{E a^2 h}{(1-\nu^2)} \iint \left[\epsilon_x^2 + \epsilon_\theta^2 + 2\nu\epsilon_x\epsilon_\theta + \frac{1-\nu}{2}\gamma_{x\theta}^2 \right] dx d\theta \tag{52}$$

21

$$u_b = \frac{Eh^3}{24(1-\nu^2)} \iint \left[\eta_x^2 + \eta_\Theta^2 + 2\nu\eta_x\eta_\Theta + 2(1-\nu)\eta_{x\Theta}^2 \right] dx\,d\Theta \tag{53}$$

From (Ref 1:676

$$\Omega = a^3 \int\limits_{-\frac{L}{D}}^{\frac{L}{D}} \int\limits_{0}^{2\pi} \left[-w + \frac{1}{2}\left(w^2 + 2\nu\frac{\partial w}{\partial \Theta} + \nu^2 - w\frac{\partial u}{\partial x} + u\frac{\partial w}{\partial x} \right) \right] \rho\,d\Theta\,dx \tag{54}$$

where

$$\epsilon_x = u_x + K_x + \frac{1}{2}\mu_x^2 \tag{55}$$

$$\epsilon_\Theta = v_\Theta - w + \iota_\Theta - \mu + \frac{1}{2}\left(\iota + \mu_\Theta \right)^2 \tag{56}$$

$$\gamma_{x\Theta} = u_\Theta + v_x + K_\Theta + \iota_x + \mu_x(\iota + \mu_\Theta) \tag{57}$$

$$\eta_x = w_{xx} + \mu_{xx} \tag{58}$$

$$\eta_\Theta = w_{\Theta\Theta} + w + \mu_{\Theta\Theta} + \mu \tag{59}$$

$$\eta_{x\Theta} = w_{x\Theta} + \mu_{x\Theta} \tag{60}$$

where ϵ_x, ϵ_Θ and $\gamma_{x\Theta}$ are strains in the shells mid-plane and η_x, η_Θ $\eta_{x\Theta}$ are the curvatures of the shell's mid-plane. In addition, u,v,w represent the dimensionlless components of the displacement vector defining the equilibrium condition before buckling occurs. Also K, ι, μ are the virtual displacements of the shell. Equations (55) to (60) are derived with the assumption of thin shells which implies that the pre-buckling rotations of the shell elements, w_x and $(v_x + w_\Theta)$ are small. Accordingly the following series representations are given for u, v, w, K, ι, μ

22

$$u = \frac{P_o}{\pi E} \sum_{n=1,3}^{\infty} \frac{\nu L}{2n\pi} X_n \sin \frac{n\partial \pi}{L} x \;+\; \frac{P \cos \theta}{\pi E} \sum_{n=1,3}^{\infty} U_n \sin \frac{n\partial \pi}{L} x \qquad (61)$$

$$v = \frac{P_i}{\pi E} \sin \theta \sum_{n=1,3}^{\infty} V_n \cos \frac{n\partial \pi}{L} x \qquad (62)$$

$$w = \frac{P_o}{\pi E} \sum_{n=1,3}^{\infty} X_n \cos \frac{n\partial \pi}{L} x \;+\; \frac{P \cos \theta}{\pi E} \sum_{n=1,3}^{\infty} Y_n \cos \frac{n\partial \pi}{L} x \qquad (63)$$

$$K = \sum_{\substack{J=1,3,5}}^{\infty} \sum_{\substack{k=2,3,4}}^{\infty} U_{jk} A_{jk} \sin \frac{j\partial \pi}{L} x \cos k\theta \qquad (64)$$

$$L = \sum_{\substack{J=1,3,5}}^{\infty} \sum_{\substack{k=2,3,4}}^{\infty} V_{jk} A_{jk} \cos \frac{j\partial \pi}{L} x \sin k\theta \qquad (65)$$

$$\mu = \sum_{\substack{J=1,3,5}}^{\infty} \sum_{\substack{k=2,3,4}}^{\infty} A_{jk} \cos \frac{j\partial \pi}{L} x \sin k\theta \qquad (66)$$

Both U_n and V_n can be expressed in terms of Y_n by use of the two differential equations expressing equilibrium in the mid-plane of the shell (Ref 1:677)

$$\nabla^4 u = \nu w_{xxx} - w_{x\theta\theta} \qquad (67)$$

$$\nabla^4 v = (2 + \nu) w_{xx\theta} + w_{\theta\theta\theta} \qquad (68)$$

Substitution of equations (61) to (66) into equations (55) to (60) and using the energy relations (52) to (54) the expression for the second variation of the potential energy is (Ref 1:677

23

$$\delta^2 v' = \int_{-\frac{L}{D}}^{\frac{L}{D}} \int_0^{2\pi} \left\{ K_x^2 + (\iota_\theta - \mu)^2 + 2\nu K_x(\iota_\theta - \mu) + \frac{1-\nu}{2}(K_\theta + \iota_x)^2 \right.$$

$$+ \frac{h^2}{12\,d^2}\left[\mu_{xx}^2 + (\mu_{\theta\theta} + \mu)^2 + 2\nu\mu_{xx}(\mu_{\theta\theta} + \mu) \right.$$

$$\left. + 2(1-\nu)\mu_{x\theta}^2 \right] + \upsilon_x\left[\mu_x^2 + \nu(\iota + \mu_\theta)^2 \right]$$

$$+ (v_\theta - w)\left[(\iota + \mu_\theta)^2 + \nu\mu_x^2 \right] + \mu_x(1-\nu)(\iota + \mu_\theta)(\upsilon_0 + v_x)$$

$$\left. + \frac{(1-\nu^2)d}{Eh}\left(\mu^2 + 2\iota\mu + \iota^2 - K_x\mu + K\mu_x \right)p \right\} dx\,d\theta \tag{69}$$

where

$$v' = \frac{2(1-\nu^2)}{Eha^2} v \tag{70}$$

Assuming a pressure distribution

$$p = p_o + p_i \cos\theta \tag{71}$$

The results of a graphical solution for equation (69) are presented in Figure 4. These curves are for peak pressures, at $\theta = 0$, which result in buckling of the shell. Thus

$$p = p_o + p_i \tag{72}$$

and the non-uniform pressure distribution described by the parameter ψ defined as (Ref 10:1)

$$\psi \;=\; \frac{P_i}{P_o + P_i} \qquad\qquad (73)$$

The curves in Figure 4 are for $E \simeq 1000\,\sigma_y$ where σ_y is the yield stress in pure tension (Ref 11:12).

FIGURE 4
Static Buckling Loads
Ref (11:27)
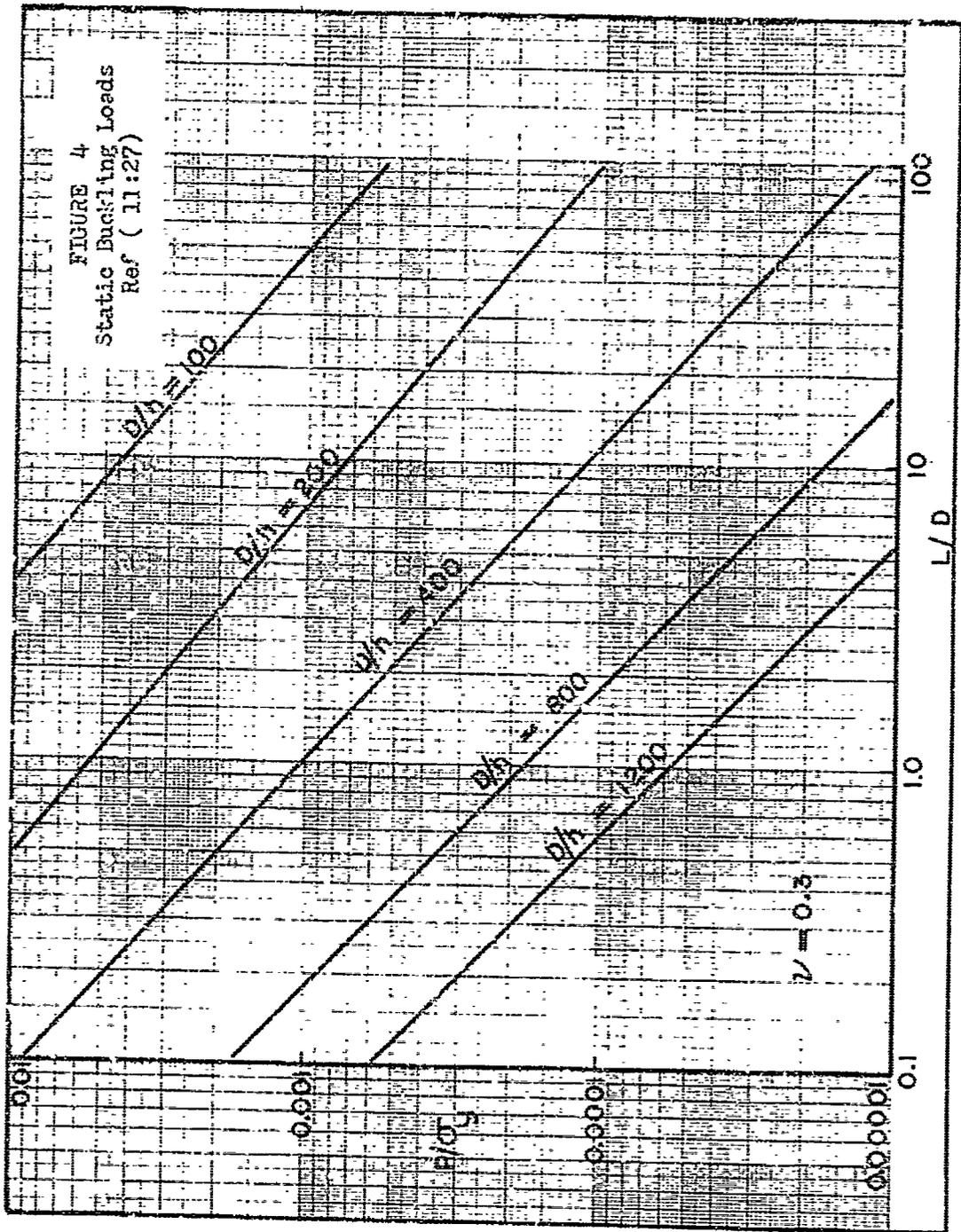
Dynamic Collapse Theory

This theory is developed using an energy analysis and an approximate deflection shape. The derivation makes use of the principle of minimum potential energy which is based on the notion of virtual work. This approach yields a system of nonlinear, coupled differential equations in the time varying coefficients of the deflection shape. Instability is predicted when these coefficients increase in time without bound (Ref 3:6). In this paper instability is assumed to occur whenever the maximum moment applied to the shell by the blast exceeds the critical maximum moment predicated by Brazier's analysis (Ref 6:109).

It is assumed that the moment-curvature relation for pure bending is valid at each cross-section and is given by (Ref 3:11)

$$M = -EI(\eta - \beta\eta^3) \qquad (74)$$

where

$$\beta = 1.5a^4(1 - \nu^2) / h^2 \qquad (75)$$

$$\eta = Y_{xx} - \frac{3}{2}Y_{xx}Y_x^2 \qquad (76)$$

where

$$Y(x,t) = \sum_{n=1}^{\infty} A_n(t)(1 - \cos\frac{2n\pi}{L}x) \qquad (77)$$

is the assumed deflection shape of the center line of the shell.

The basis of this analysis, as mentioned previously, is the principle of virtual work which can be formulated as:

> If an elastic body in a dynamic state is subjected to
> a variation of its deformation at a fixed time, the
> change in strain energy equals the increment of work
> of the surface, body, and inertial forces (Ref 3:11).

Assuming that there are no body forces, the strain energy can be

written as

$$U = \frac{EI}{2} \int_0^L (\eta^2 - \frac{\beta}{2} \eta^4) \, dx \qquad (78)$$

Substitution of equation (76) into equation (78) and taking the first variation, equation (78) becomes

$$\delta U = EI \int_0^L \left[\left(Y_{xx} - 3Y_x^2 Y_{xx} - \beta Y_{xx}^3 \right) \delta(Y_{xx}) - 3Y_x Y_{xx}^2 \delta(Y_x) \right] dx \qquad (79)$$

The expression for the virtual work of the inertia forces is

$$-\int_{vol} \rho \ddot{\bar{u}} \cdot \delta \bar{u} \, d(vol) = -\zeta \int_0^L \left[Y_{tt} \delta Y + \frac{5}{2}\eta^2 \left(Y_{txx}^2 + Y_{xx} Y_{ttxx} \right) Y_{xx} \delta Y_{xx} \right] dx \qquad (80)$$

where u represents the deformation state, the dots represent differentiation with respect to time, ζ is the mass density per unit length, and

$$\eta = a^5 (1 - \nu^2) / h^2 \qquad (81)$$

Equations (79) and (80) include terms thru only the fourth order in Y and its derivatives.

Since only ovalization terms due to longitudinal bending have been considered and since equation (79) has no contribution due to the ovalization effect of the external pressure, it is consistent to omit the corresponding contribution in the virtual work expression (Ref 3:13).

Only the virtual work of the center line deflection due to the external pressure is included. Thus

$$\int_S \overline{F} \cdot \overline{u} \, dS = \int_S p \cos\theta \, \delta Y \, dS \qquad (82)$$

where

$$p = p_r \cos\theta \, e^{-\Gamma t} \quad , \quad -\frac{\pi}{2} \leq \theta \leq \frac{\pi}{2} \qquad (83)$$

$$p = 0 \quad , \quad \frac{\pi}{2} \leq \theta \leq \frac{3\pi}{2} \qquad (84)$$

p_r is the peak reflected pressure and Γ is the decay parameter and defined as p_r/I_r. Substituting (83) into (82)

$$\int_S p \cos\theta \, \delta Y \, dS = \frac{\pi}{2} p_r \, a \, e^{-\Gamma t} \int_0^L \delta Y \, dx \qquad (85)$$

Using a single term approximation, the deflection shape is

$$Y(x,t) = A_1(t)\left(1 - \cos\frac{2\pi x}{L}\right) \qquad (86)$$

Then, by performing the appropriate differentiation on equation (86) as required in equation (79) the variation in the strain energy becomes

$$\delta U = EI\left[\frac{16\pi^4 A_1}{L^4}\left(1 - \frac{6\pi^2}{L^2}A_1 - \beta\frac{12\pi^4}{L^4}A_1\right)\right]\left(\frac{L\delta A_1}{2}\right) \qquad (87)$$

the virtual work becomes

$$\delta W_i = \left[\ddot{A}_1 + \frac{160\pi^8\eta^2}{L^8}\left(A_1\dot{A}_1^2 + A_1^2\ddot{A}_1\right)\right]\left(\frac{3L\zeta\delta A_1}{2}\right) \qquad (88)$$

and the pressure work becomes

$$\delta W_p = \left(\pi p_r a \, e^{-\Gamma t}\right)\left(\frac{L\delta A_1}{2}\right) \qquad (89)$$

Using the principle of minimum potential energy

$$\delta U - \delta W_i + \delta W_p = 0 \qquad (90)$$

28

and solving for $\ddot{A}_1$

$$\ddot{A}_1 = \frac{32 D \left(\frac{L}{D}\right)^8}{32 D^2 \left(\frac{L}{D}\right)^8 + 5\pi^8 \left(\frac{D}{a}\right)^4 (1-\nu^2)^2 A_1^2} \left\{ \left[\frac{64.4\, PRED\cdot E\, \frac{D}{a} e^{-rt}}{\rho\, 10^6} \right.\right.$$

$$+ \frac{128.8\, E\, \pi^4}{\left(\frac{L}{D}\right)^4 D^3 \rho} \left[\frac{D^2 \left(\frac{L}{D}\right)^2 - \pi^2 A_1^2 \left(6 + 0.375(1-\nu^2)\left(\frac{D}{a}\right)^2 \right)}{\left(\frac{L}{D}\right)^2} \right.$$

$$\left. \left. \frac{\left/ \left(\frac{L}{D}\right)^2\right)}{1} \right] A_1 \right] - \frac{5\pi^8 (1-\nu^2)^2 \left(\frac{D}{a}\right)^4}{32 D \left(\frac{L}{D}\right)^8} A_1 \dot{A}_1^2 \right\} \tag{91}$$

where

$$PRED = \frac{p_r}{E} \times 10^6 \tag{92}$$

Equation (91) is solved using a Runge-Kutta method coupled with an Adams-Bashforth and Adams-Moulton predictor-corrector scheme (Ref 12). This scheme has provisions for varying the time increment and allows for variations in the shell sizes. A copy of this program is contained in Appendix A along with the appropriate information needed for operation.

The maximum moment, at any given time, occurs at the ends of the cylinder. For the case of interest, however, the hinge collapse line forms approximately at the middle of the shell. Thus the maximum moment in the expressions below is that value of the moment at the middle of the shell. Using equations (74) thru (77) and the condition $\theta = 0$,

this moment is

$$M_{max} = \pi E I A_1 L^2 (1 - \beta A_1^2 L^4) \qquad (93)$$

Recall

$$I = \frac{\pi (D^4 - d^4)}{64} \approx \frac{\pi D^4}{16(D/h)} \qquad (94)$$

for

$$D/h \geq 100 \qquad (95)$$

where

$$d^4 = (D-h)^4 = D^4(1 - \frac{h}{D})^4 \qquad (96)$$

Then

$$M_{max} = -\frac{\pi^3 E D^2 A(t)}{4(D/h)(L/D)^2} \left[\frac{1.5 \pi^4 (D h)^2 A_1^2(t)}{(1-\nu^2) D^2 (L/D)^4} - 1 \right] \qquad (97)$$

To determine if a shell under a particular blast loading will fail or not involves the following process:

1. Determine Brazier's collapse moment from

$$M_c = \frac{0.4935 E D^3}{(\frac{D}{h})^2 \sqrt{1-\nu^2}} \qquad (98)$$

2. Use the computer program (Appendix A) to solve equation (91) for the time history of $A_1(t)$ and the bending moment, M_{max}.

3. Find the time at which the moment, M_{max}, reaches a maximum.

4. If the time is less than 0.160 sec and M_{max} is greater than Brazier's collapse moment, then the shell will collapse.

30

Static Collapse Theory

Two approaches were used in the static collapse situation. The first approach failed due to the difficulty in solving the governing equations of motion (see Appendix B). The second method used by Greenspon (Ref 10), yields only an upper bound to the dynamic iso-damage curves. This fact is seen in Figure 5.

The first approach taken utilizes the force-equilibrium equations from shell theory. These equations are given by Timoshenko (Ref 14), and are generalized to include the end effects and asymmetric pressure loadings. The development of these equations for shells of finite length (short as well as long) is in Appendix B. A computer program for shells of L/D ratios > 15 is also given in Appendix B.

The second approach taken follows that presented by Greenspon (Ref 10). The pressure loading corresponds to the pressure parameter $\psi = 0.5$, where ψ is defined as

$$\psi = \frac{P_i}{P_i + P_o} \tag{99}$$

Assuming that membrane theory holds, and that the pressure distribution can be expressed as

$$p = p_o(1 + \frac{P_i}{P_c} \cos \theta) = p_o f(\theta) \tag{100}$$

the membrane force resultants can then be written as

$$N_\theta = a p_o f(\theta) \tag{101}$$

$$N_{x\theta} = -p_o x \frac{\partial f(\theta)}{\partial \theta} \tag{102}$$

$$N_x = \frac{p_o}{a} \frac{x^2}{2} \frac{\partial^2 f(\theta)}{\partial \theta^2} + \nu a p_o f(\theta) - \frac{p_o}{a} \frac{L^2}{24} \frac{\partial^2 f(\theta)}{\partial \theta^2} \tag{103}$$

At the center of the shell, $x = L/2$, $0 = 0$, equations (100) thru (103) reduce to

$$p = p_o + p_i \tag{104}$$

$$N_\theta = ap \tag{105}$$

$$N_{x\theta} = 0 \tag{106}$$

$$N_x = p\left(a\nu - \frac{L^2}{24}\psi\right) \tag{107}$$

Using Von Mises yield condition

$$N_x^2 - N_x N_\theta + N_\theta^2 + 3N_{x\theta}^2 = (\sigma_y h)^2 \tag{108}$$

where σ_y is the yield stress in pure tension and h is the shell thickness, the critical pressure for collapse is

$$(p)_c = \sigma_y \frac{h}{a} \frac{1}{\sqrt{(1-\nu+\nu^2) + \psi(1-2\nu)\left(\frac{L^2}{12a^2}\right) + \psi^2\left(\frac{L^2}{12a^2}\right)^2}} \tag{109}$$

For $\psi = 0.5$ and $\nu = 0.3$, equation (109) reduces to

$$\frac{(p)_c}{\sigma_y} = \frac{h}{D} \frac{2}{\sqrt{0.79 + 0.0416\left(\frac{L}{D}\right)^2 + 0.0001085\left(\frac{L}{D}\right)^2}} \tag{110}$$

The results of equation (110) are shown graphically in figure 6 for various L/D and D/h ratios.

FIGURE 5
Comparison of Theory (Ref 6) to
Experimental data (Ref 13) for
collapse-hinge failure

x = denotes experimental data
    for shells 33-36 (Ref 13)

FIGURE 6
Static Collapse Loads
Ref(11 #27)
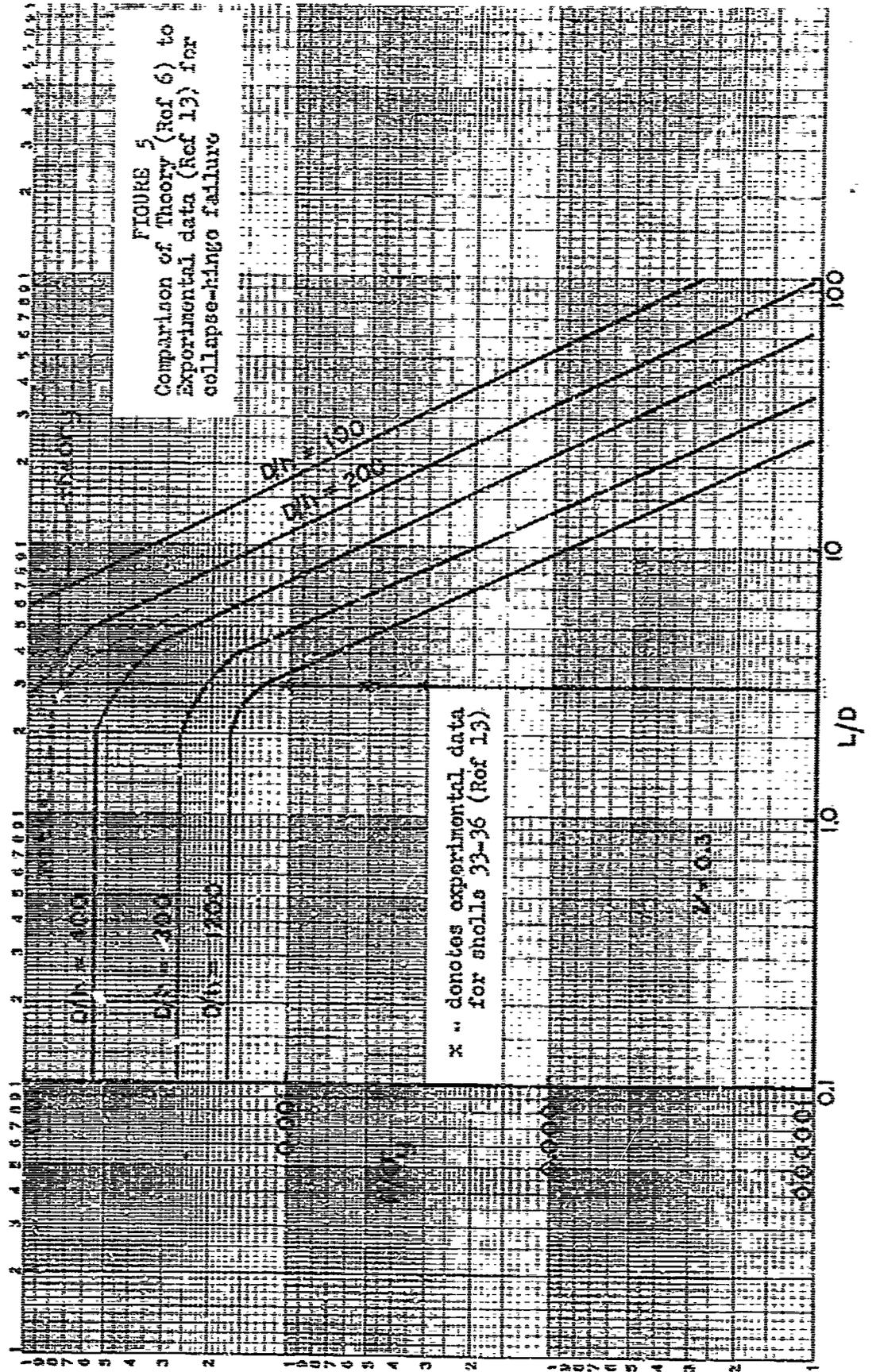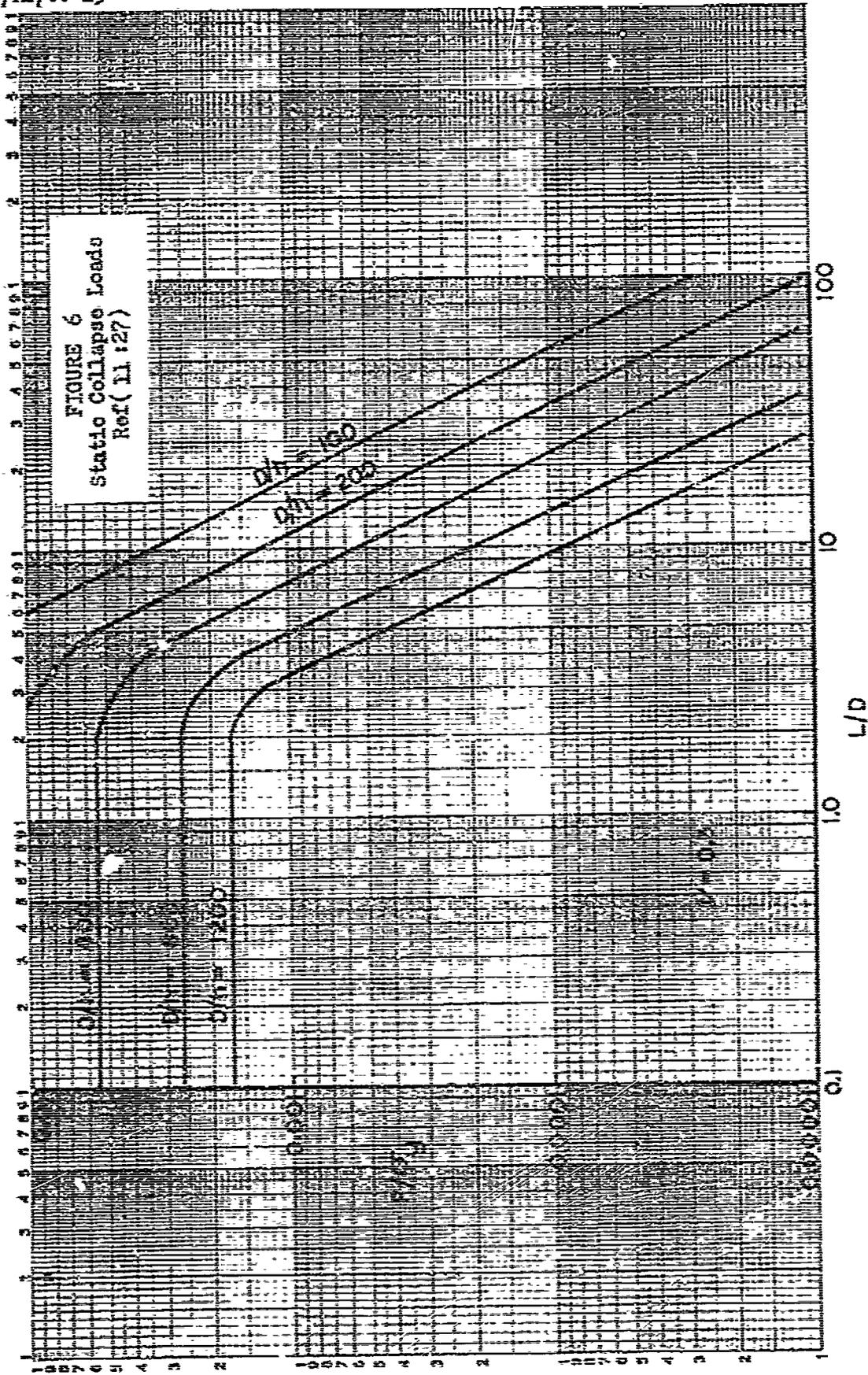
V. Determination of Critical Shell Parameters

To determine the critical shell parameters it is first necessary to construct a family of iso-damage curves. The equations that are used to construct the iso-damage are summarized first. The results of a study of these curves for different materials are then discussed.

The characteristic damaged shape for the buckling mode is indicated in Figure 7. Let the asymptotes of the tangent-modulus branch and elastic branch be represented by I_T, P_T and I_E, P_E respectively.

The value of P_T from numerical integration of equation (16) (Ref 2:232) is

$$P_T = \frac{3}{4} \sigma_y \left(\frac{h}{a}\right) \tag{111}$$

where σ_y is the yield stress.

The value of I_T can be estimated by assuming $\sigma_\ominus$ and E_t are constant during the plastic flow phase of buckling. The amplitude of the nth. flexural mode can be expressed by use of equation (24) where $\Upsilon_y = 0$. Thus

$$w_n(\mathcal{T}) = \dot{w}_n(0) \frac{\sinh q_n \mathcal{T}}{q_n} \tag{112}$$

The most amplified mode is the one having the largest q_n and is determined by substituting equation (26) into (25). Thus

$$q_n\Big|_{max} = \frac{\sigma_y}{2 E_t a} \left(\frac{E_t}{E}\right)^{\frac{1}{2}} \tag{113}$$

where $\gamma/2$ is considered small compared to unity and $\sigma_\ominus$ has been replaced by σ_y in accordance with the assumption $\sigma_\ominus$ remains constant (Ref 2:236). Assuming that an amplification factor of 1,000 produces

buckling, $q_n\big|_{max}$ can be expressed as (Ref 2:236)

$$q_n\bigg|_{max} = -\frac{Bh\sigma_y}{c I_T} \qquad (114)$$

where b is a constant and c is defined as $\sqrt{E/\rho}$. Thus equating equations (113) and (114) yields

$$I_T = 2hBc\sqrt{\sigma_y \rho}\sqrt{\frac{E_t}{\sigma_y}} \qquad (115)$$

By relaxing the requirement that E_t remain constant, equation (115) can be brought into closer agreement with the actual situation. Thus let E_t be represented by

$$E_t = \frac{\sigma}{K(\epsilon - \epsilon_y)} \qquad (116)$$

where the slope of the stress-strain plot of σ/E vs percent strain, ϵ , defines the value of K. By equating the kinetic energy imparted by the impulse, I_T, to the strain energy absorbed in plastic work, equation (115) may be replaced by

$$I_T = \left(\frac{95}{K}\right)^{\frac{1}{4}}\left(\frac{h}{a}\right)^{\frac{3}{2}}\left(\sigma_y \rho\right)^{\frac{1}{2}} a \qquad (117)$$

where B is assigned the value 12 to match the numerical integration with an amplification of 1,000 (Ref 2:238).

P_E is determined from equation (45) as the smallest critical value and for $Z = .3$ is (Ref 2:233) given by

$$P_E = 0.92 E\left(\frac{a}{L}\right)\left(\frac{h}{a}\right)^{\frac{5}{2}} \qquad (118)$$

The value of I_E from (Ref 2:233) is

36

$$I_E = 5 a \sqrt{\frac{}{\cdot \rho}} \left(\frac{h}{a}\right)^2 \qquad (119)$$

To construct the iso-damage curves, the approximate hyperbolic formula

$$\left(\frac{P}{P_A} - 1\right)\left(\frac{I}{I_A} - 1\right) = 1 \qquad (120)$$

is used (Ref 2:233). Depending on the curve branch, P_A and I_A are the values given by equations (111) or (118) and (117) or (119) respectively.

Using equations (118) and (119) the values of the asmyptotes were calculated for 1040 steel, 6061-T6 aluminum, 5052-H38 aluminum and 1100-0 aluminum. These values are tabulated in Appendix C for various L/D and D/h ratios. Solving equation (120) for I, then permits one to pick a pressure and solve for the corresponding impulse. By picking different values for the pressure and calculating the corresponding impulses, it is possible to construct a iso-damage curve for any sized shell. Proceeding in this manner, the theoretical curves in Figures 12 to 16 were constructed. Superimposed on these same Figures are the experimental iso-damage curves that were obtained by Schuman (Ref 13:43-6).
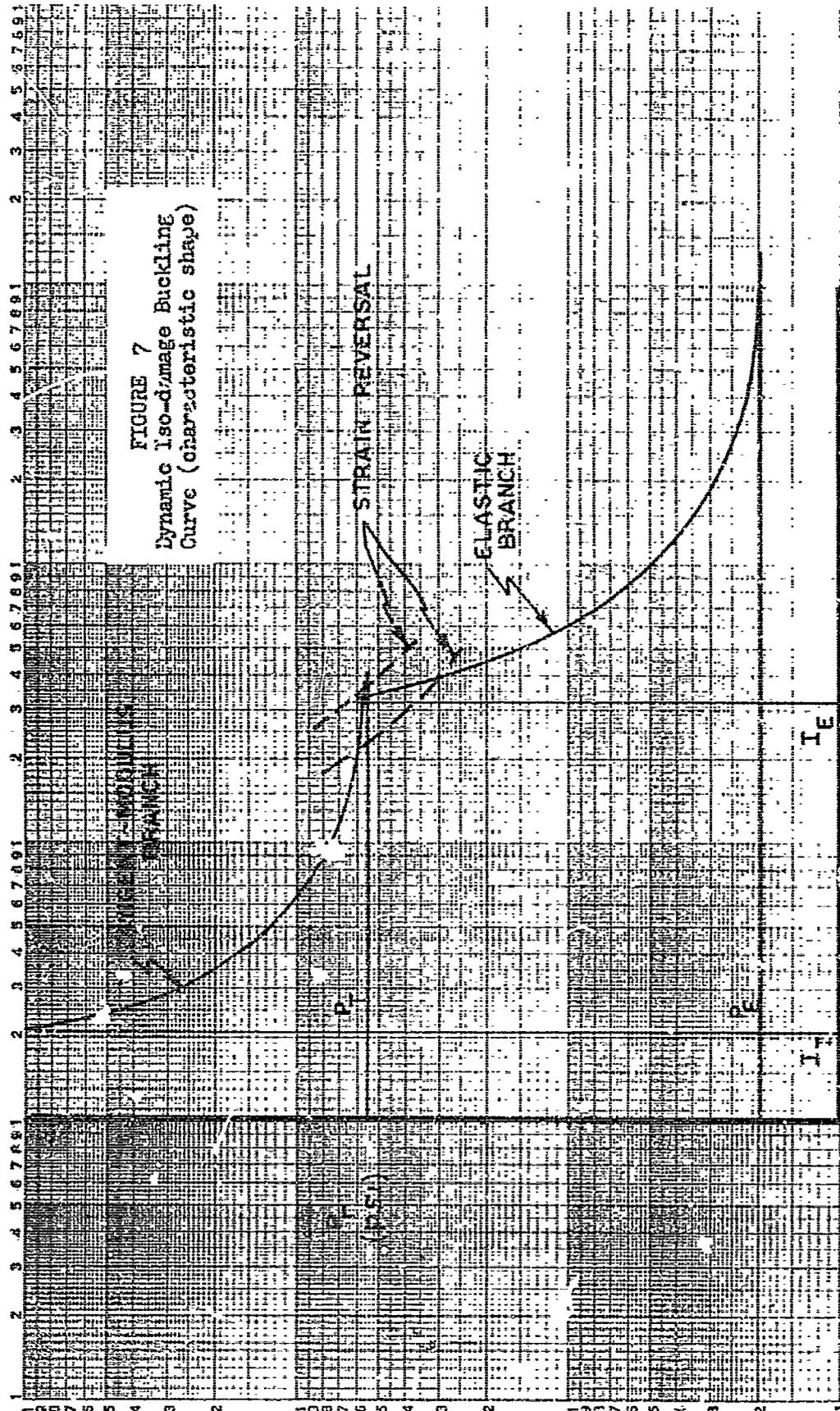
FIGURE 7
Dynamic Iso-damage Buckling
Curve (characteristic shape)

In the cases where Schuman did not test a shell of particular interest, the curves on pages 55-58 of (Ref 13) were used to calculate a critical pressure. The empirical formula for use of these curves is given by

$$P_{cr} = P_0 \, F_w \, F_D \, F_t \, F_{L/D} \qquad (121)$$

where P_0 is the atmospheric pressure and the other functions are as described on Figures 8-11. The quantities F_w, F_d, F_t, and $F_{L/D}$ are nondimensional and are scalars. Using this value of critical pressure, the curves on pages 43-46 of (Ref 13) were extrapolated to give the desired iso-damage curve.

Figures 12 to 16 present sets of iso-damage curves for the four materials investigated in this paper. The theoretical curves were constructed using the dynamic buckling theory developed in chapter 4 and the expression for the critical pressures and impulses presented by equation (120) in chapter 5. The expreimental curves ware constructed using the expreimental data generated by Schuman (Ref 13). Below is a brief discussion of each of the above figures and the trend illustrated by each figure.

FIGURE 8
Thickness Factor, F_t
Ref (13 : 58)

1. 1040 STEEL
2. 1100-0 Al
3. 6061-T6 Al
4. 5052-H38 Al

+ inches

40

FIGURE 9
Diameter Factor, F_D
Ref (13:57)

D , inches

FIGURE 10
Charge Weight Factor, F_W
Ref (13:56)

W, pounds

FIGURE 11
Length-to-Diameter Ratio Factor, $F_{L/D}$
Ref (13 :55)
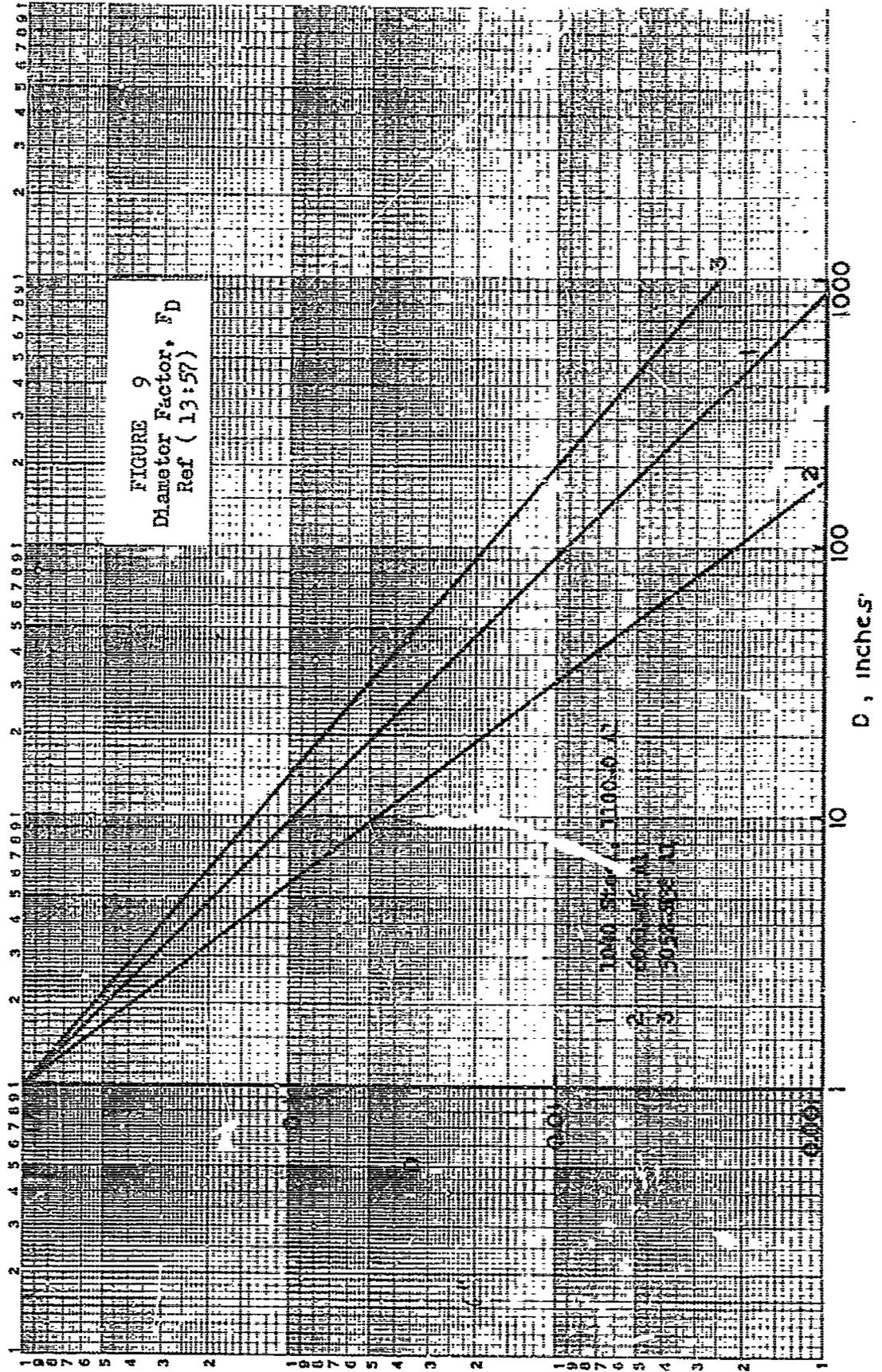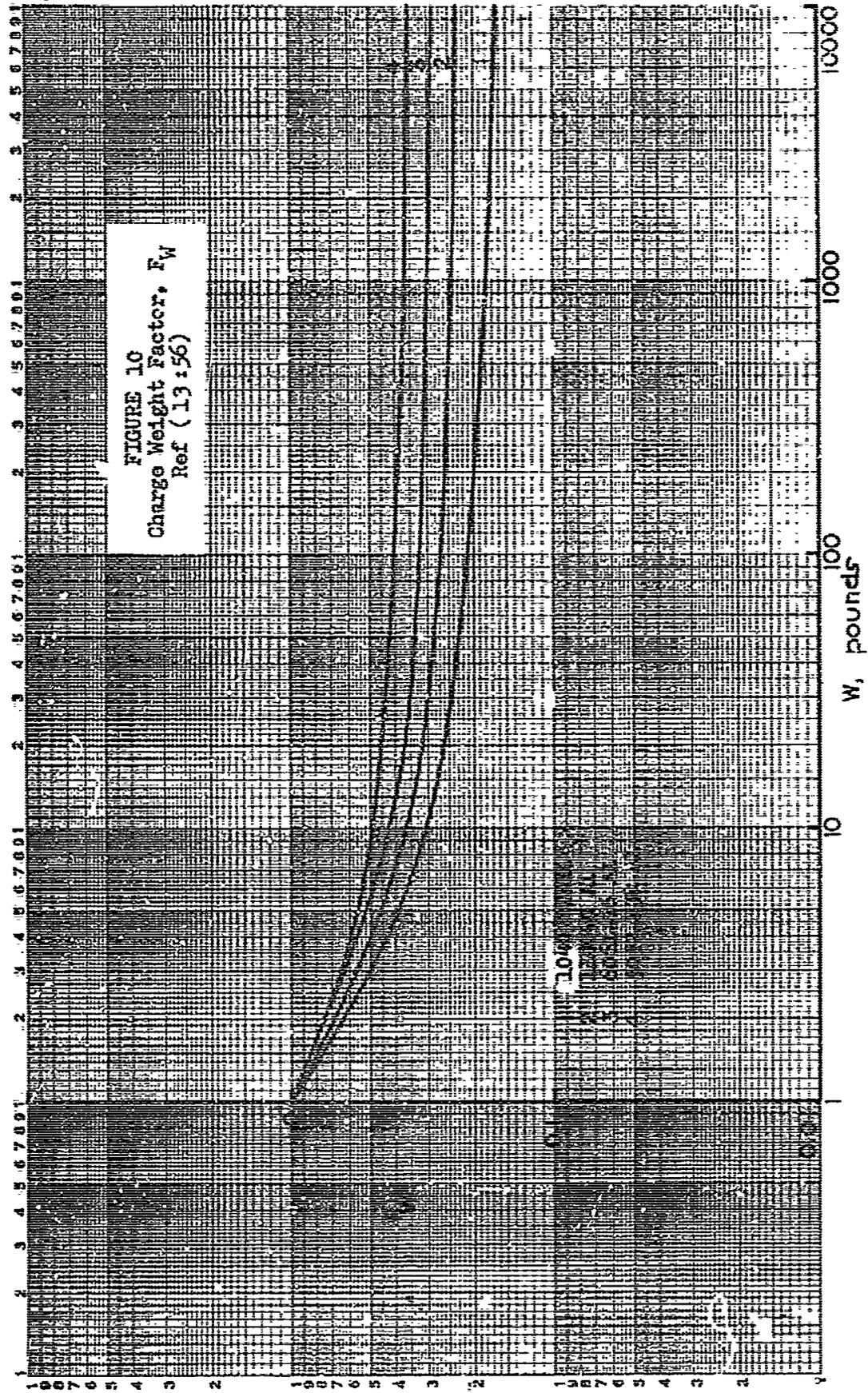
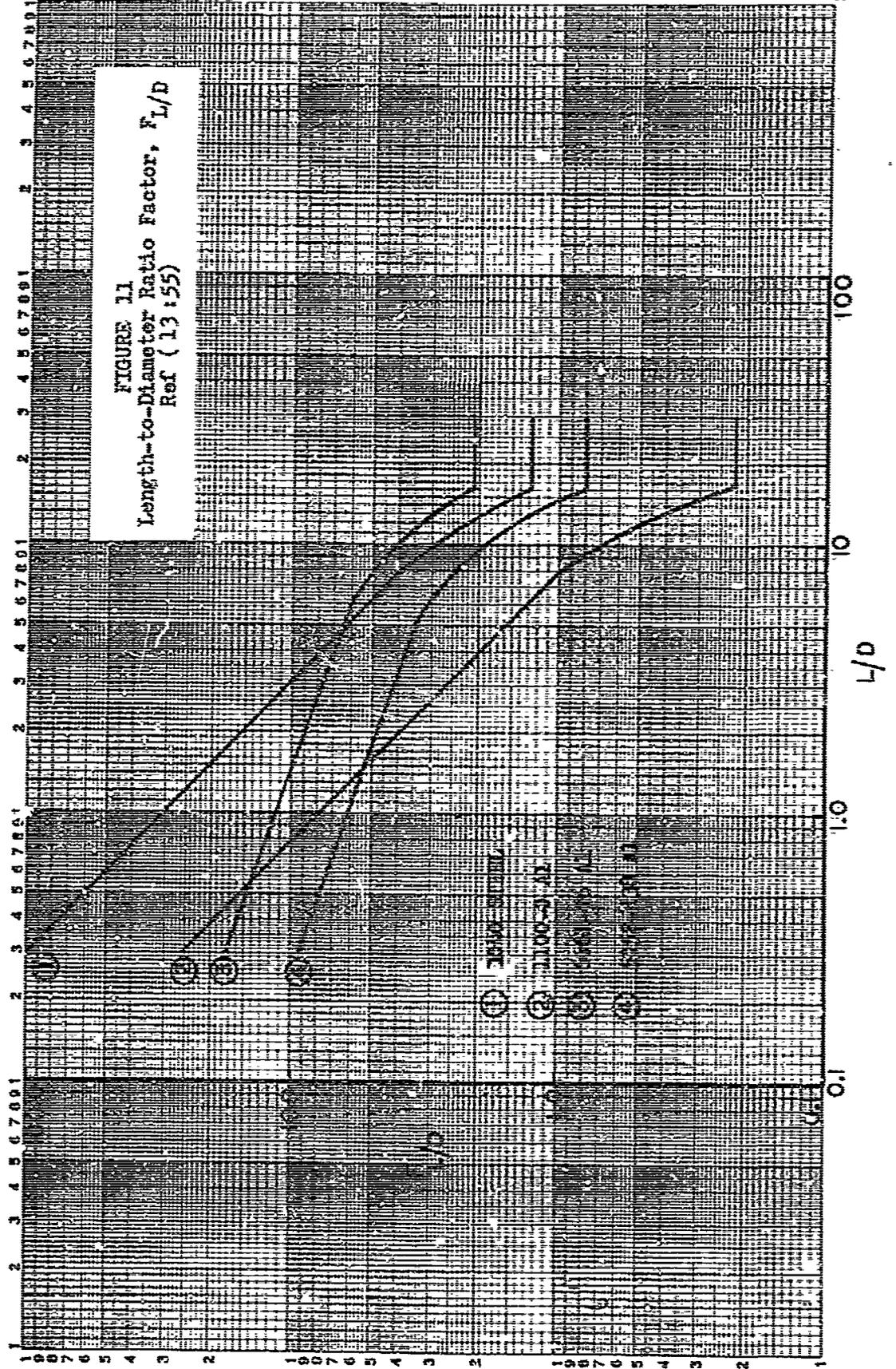Figure 12 is a set of iso-damage curves for 1040 steel. Experimental curve #1, is for shells 33-37 (Ref 13:97) which failed in the hinge collapse pattern. The experimental points scattered about curve #2 are for shells 8-16 (Ref 13:97) which failed in the hinge collapse pattern. These iso-damage curves seem to indicate that, for L/D ratios of 3 and D/h ratios in the range indicated, the dynamic buckling theory can predict failure due to the formation of the hinge collapse pattern.

Figure 13 is a set of iso-damage curves for 6061-T6 aluminum. Curve #1 is for shell 167 (Ref 13:100) which failed in the hinge collapse pattern. Curve #2 is for shell 137 which failed in the hinge collapse pattern with slight buckling. Thus this shell (#137) failed in what can be called a threshold combination pattern. These iso-damage curves also seem to indicate that, for L/D ratios of 1 and D/h ratios as indicated, the dynamic buckling theory again seems to predict failure due to the formation of both hinge collapse and combination patterns.

Figure 14 is a set of iso-damage curves for 1100-0 aluminum. Curve #1 is for shells 194-197 (Ref 13:101) which failed in a hinge collapse pattern. Curve #2 is for shells 174-179 (Ref 13:100-1) which failed in a wave buckling pattern. Curves #1, seem to indicate that for L/D ratios of 3 and D/h ratios of 250, the dynamic buckling theory does not accurately predict hinge collapse failure. This theory would, however, yield a set of critical pressures and impulses which would result in an extensive degree of damage due to the formation of the hinge collapse pattern. Curves #2 only seem to verify that if a shell fails in the wave buckling mode, the dynamic buckling theory is valid in its prediction.

Figure 15 is a set of iso-damage curves for 5052-H38 aluminum. Curve #1 is for shells 89-91 (Ref 13:98) which failed in the hinge

collapse pattern. Curve #2 is for shells 92-94 (Ref 13:99) which also failed in the hinge collapse pattern. Curve #3 is for shells 76-84 (Ref 13:98) which failed in the combination pattern. Curves #1 and 2 seem to indicate that, for L/D ratios of 2 and 3 and for D/h ratios of 375, the dynamic buckling theory can predict failure due to the formation of the hinge collapse pattern. Curves #3 and D/h ratios of 500, the dynamic buckling theory cannot accurately predict failure due to the formation of the combination pattern.

Figure 16 is a set of iso-damage curves for 5052-H38 aluminum. Curve #1 is for shells 123-128 (Ref 13:99) and L/D of 3 which failed in the combination pattern. Curve #2 is for shell 68 (Ref 13:99) and L/D of 5 which also failed in the combination pattern. For these shells, note that they virtually form the same iso-damage curve and that they failed in the same mode. The dynamic buckling theory, however, differs radically from the experimental results and in addition, differs for the L/D ratios. Hence, the dynamic buckling theory cannot accurately predict failure for the L/D and D/h ratios indicated when the shell fails due to the formation of a pattern different than that of wave buckling.

Based on the above analysis of Figures 12 to 16, it is concluded that the L/D ratio is not the most important parameter in determining the failur pattern of the shells investigated. In addition, the dynamic buckling theory can predict failure due to the formation of the hinge collapse and combination patterns only for low and moderate D/h ratios, but can accurately predict failure for the wave buckling pattern. Proceeding on this basis, Figures 17 to 28 were constructed by holding the L/D ratio constant and allowing the D/h ratio to vary. In this manner, a limiting value on the D/h ratios can be indicated such that the valid range for the theories presented in chapter 4 can be established.

This analysis will also predict which failure pattern is to be expected given an L/D ratio, a D/h ratio, and a critical reflected pressure.

Assuming that the D/h ratio is the critical shell parameter in determining the failure mode, estimates were made by this researcher as to which failure pattern would appear and at which critical pressure. These shells were then fired by Schuman at BRL laboratories in Maryland. The results of these firings are presented in Appendix D. For clarity, however, a brief discussion will be presented below.

The first three figures of Appendix D are for 1100-0 Al. The failure pattern's obtained were as predicted, ie the collapse pattern for moderate D/h ratios (275) and the combination pattern for slightly higher D/h ratios (375-400). This information coupled with data from Reference 13, pages 100-101, shells #174-181, illustrate the complete range of failure modes. Shells #174-181 having failed in the wave buckling pattern with shell parameters of $L/D = 1$ and $D/h = 500$.

The last two figures of Appendix D are for 5052-H38 Al. The failure patterns obtained were as predicted, ie the wave buckling pattern for high D/h ratios (750-1000). Note that even though the L/D ratios were radically different (0.333 and 3.0), the same failure pattern was observed for these high D/h ratio's.

FIGURE 12
Iso-Damage Curves
1040 Steel

1 L/D = 3, D/h = 316, D = 3

2 L/D = 3, D/h = 158, D = 3

I_r, psi - msec

FIGURE 13
Iso-Damage Curves
6061-T6 Al

1 L/D = 1, D/h = 119, D = 3in
2 L/D = 1, D/h = 136, D = 7.5

FIGURE 14
Iso-Damage Curves
1100-0 Al

1	L/D = 3,	D/h = 250,	D = 3
2	L/D = 3,	D/h = 500,	D = 3

I_r , psi-msec

FIGURE 15
Iso-Damage Curves
5052-H38 Al

1	L/D = 3,	D/h = 375,	D = 3in
2	L/D = 2,	D/h = 375,	D = 3in
3	L/D = 3,	D/h = 500,	D = 3in

I_r)   psi-msec

FIGURE 16
Iso-Damage Curves
5052-H38 Al

1	L/D = 3,	D/h = 1000,	D = 6in
2	L/D = 5,	D/h = 1000,	D = 6in

$O, \triangle$ — experimental

I_r, psi-msec
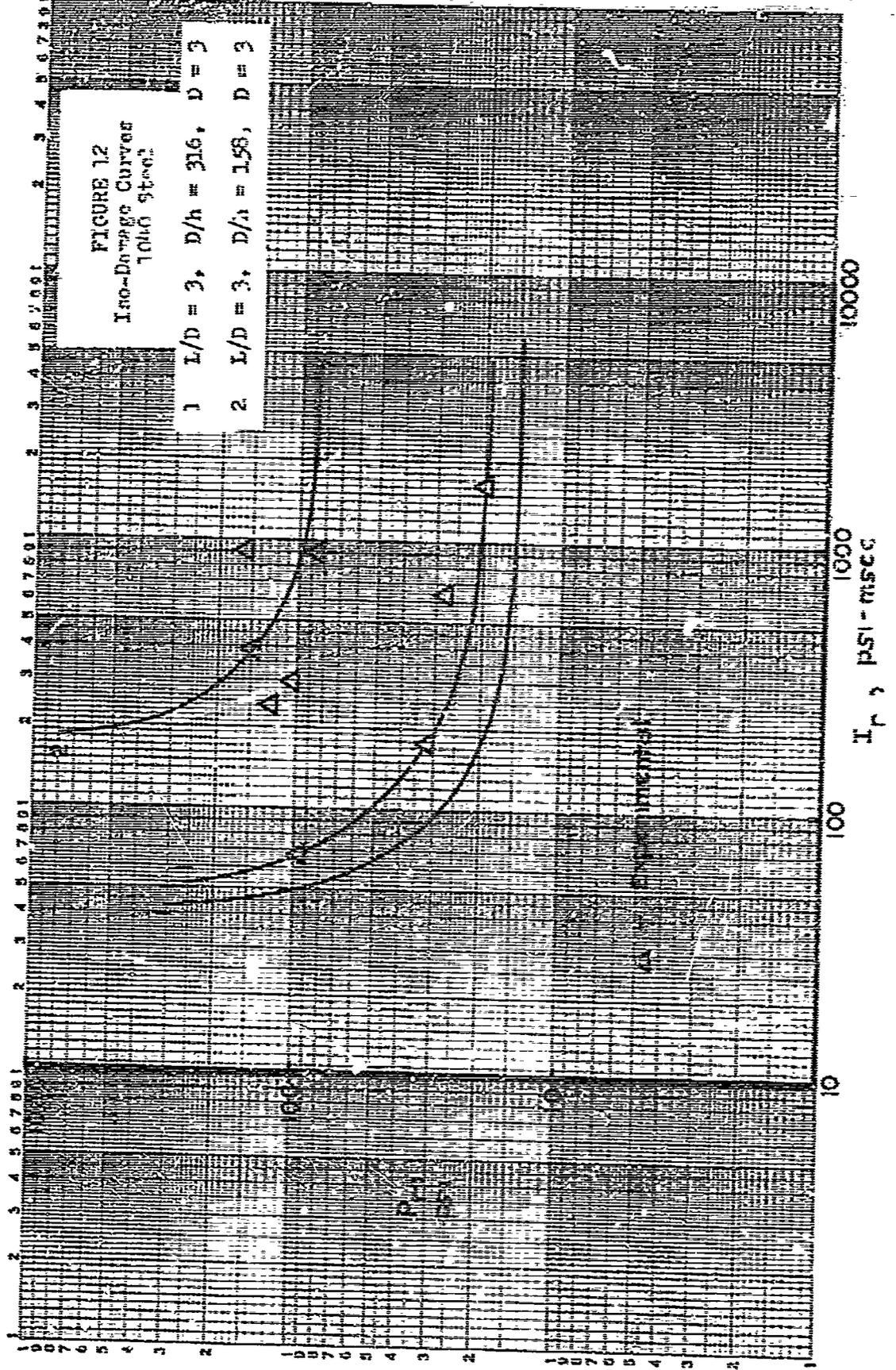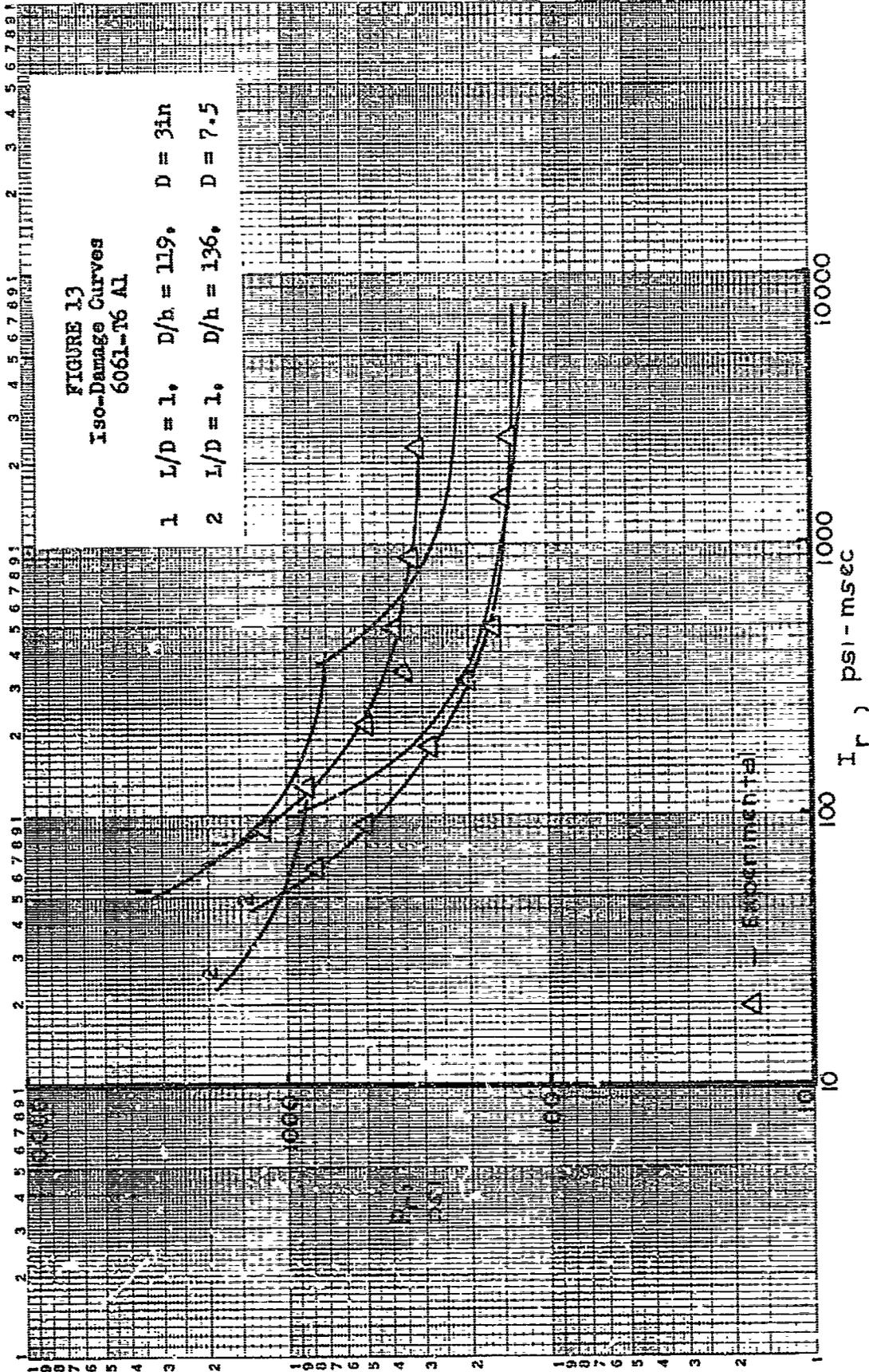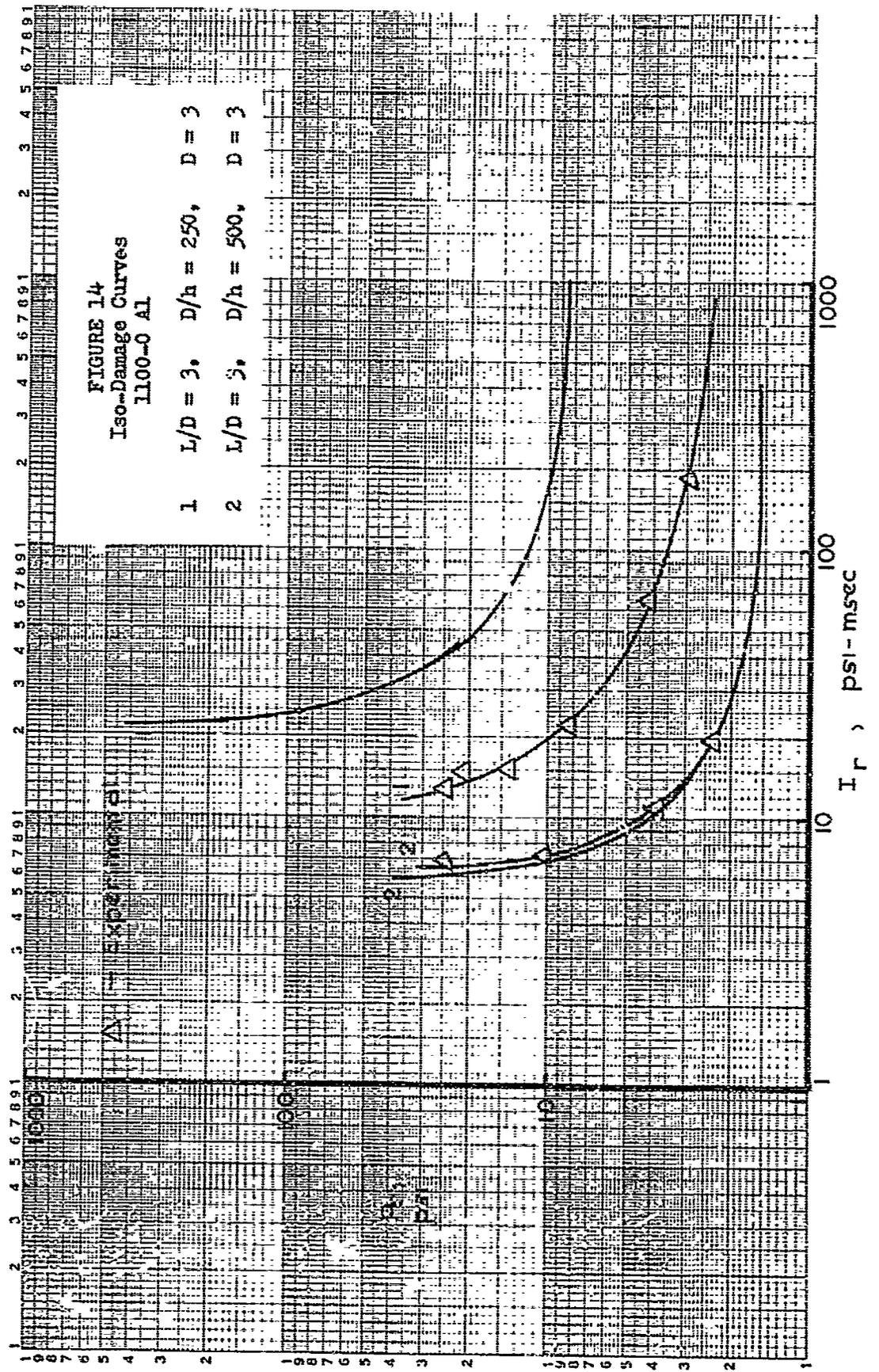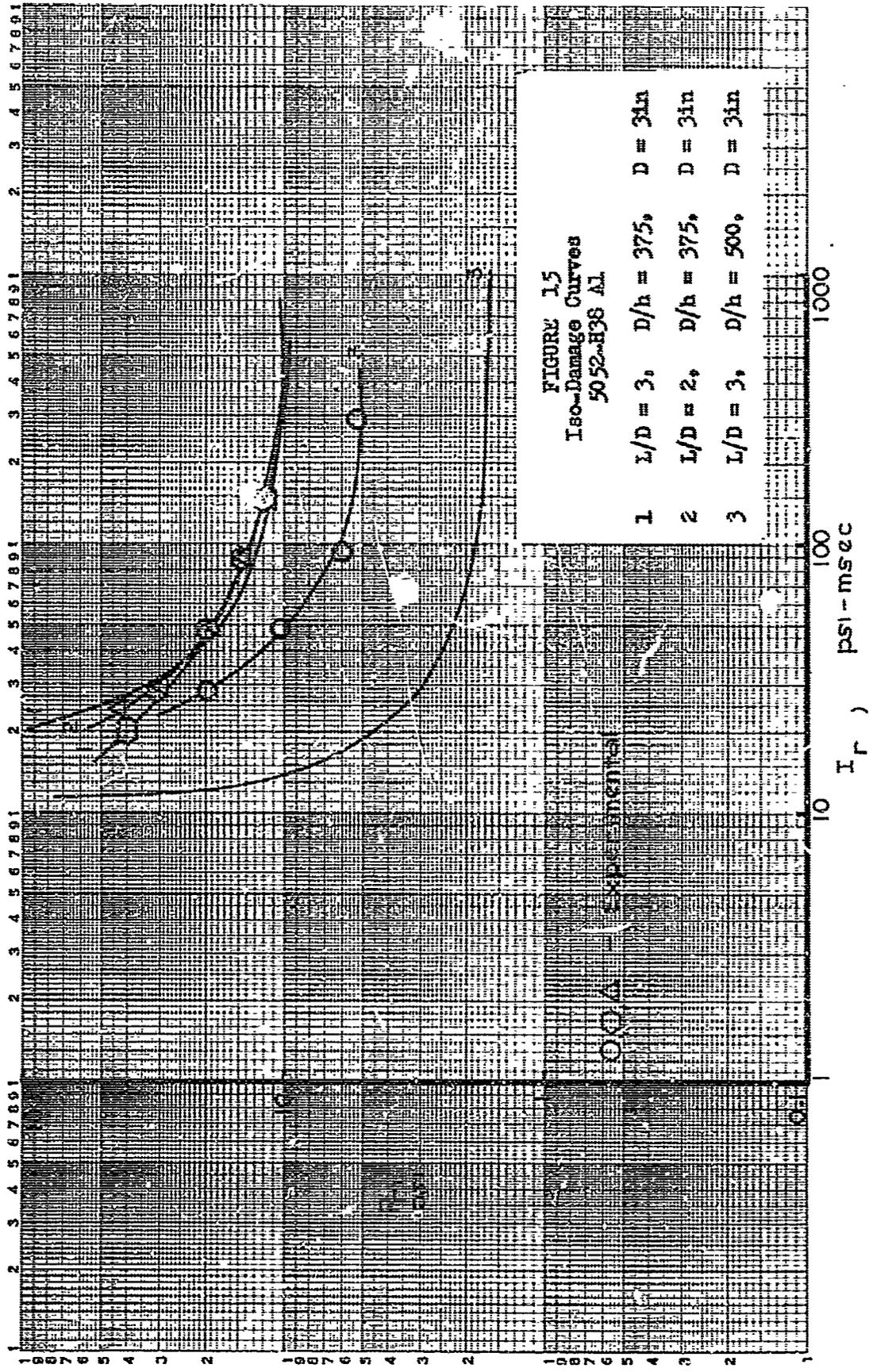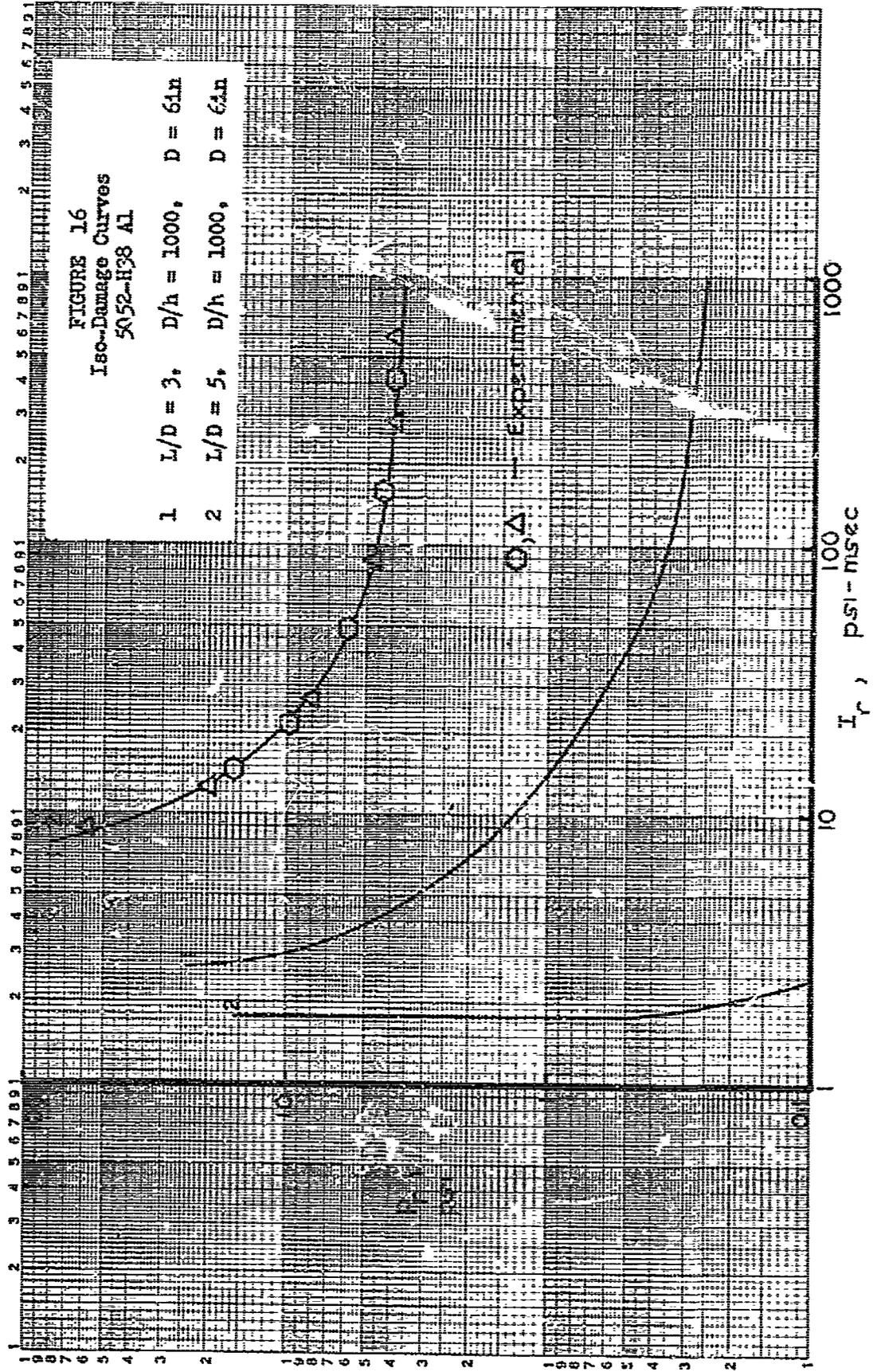
As mentioned on page 29, a program was written to numerically integrate equation (91). The results of this program were not conclusive. The solution for $A_1(t)$ and M_{max} was found for a PRED values between 10 and 30 and a decay parameter (Γ) between 9.5 and 11.1. The value of $A_1(t)$ and M_{max} thus obtained could not be duplicated for identical input data. This discrepancy is believed due to the integration step size. Hence the step size was reduced, but no output could be obtained from the program. By modifing the program, intermedicate results were obtained. The results indicated that the maximum moment generated never exceeded Brazier's collapse moment. The coefficient, $A_1(t)$, was also found to be oscillatory. Increments on PRED still did not produce a large enough moment. A possible explanation for this is that the value of Γ may be to large. This large valve of Γ was assumed such that regions of high pressure and low impulses were investigated. The reason being that this area corresponded to a similar area generated by the dynamic buckling theory. For these reasons, no theoretical dynamic collapse curves are presented on Figures 17-28. Perhaps a value of Γ between 0.1 and 2 0 will yield useful dynamic collapse curves.

Below is a short discussion of Figures 17-28 and the importance of each. The curves were constructed using the static and dynamic theories presented in chapter four of this paper. The conclusions drawn from these figures are based on the assumption that the limiting value of the D/h ratio is that value where the two static curves and two dynamic curves intersect each other. That is, one value is obtained where the static curves intersect and likewise for the dynamic curves.

Figures 17-19, which are for 1040 steel, indicate that the lower transition value at D/h is between 90 and 130.

Figure 18 indicates that the upper transition value of D/h is approximately 435.

Figures 20-22, which are for 6061-T6 aluminum, indicate that the lower transition value of D/h is between 90 and 130.

Figures 23-25, which are for 5052-H38 aluminum, indicate that the lower transition value of D/h is between 90 and 135.

Figure 24 indicates that the upper transition value of D/h is approximately 455.

Figures 23-25, which are for 5052-H38 aluminum, indicate that the limiting D/h ratio is between 90 and 130.

Figure 27 indicates that the upper transition value of D/h is approximately 460.

Since the lower transition value of D/h is the same for each of the four materials investigated, assume an average value of 110. Since L/D did not seem to affect the lower transition point, assume that it does not affect the upper transition point. Hence from Figures 18, 24, and 27 this upper transition value is approximately at the value of D/h = 450. Now the failure modes can be broken down into three areas. From D/h = 0 to 110, the hinge collapse pattern should be dominant. From D/h = 100 to 450, the combination pattern should be dominant. From D/h above 450, the wave buckling pattern should be dominant.

FIGURE 17
Critical Pressure Parameter
vs
D / h

1   Static Buckling
2   Dynamic Buckling
3   Static Collapse
4   Dynamic Collapse

1040 Steel   L/D = 1

FIGURE 18
Critical Pressure Parameter
vs
D / h

1   Static Buckling
2   Dynamic Buckling
3   Static Collapse
4   Dynamic Collapse

1040 Steel   L/D = 3

O—Experimental

$\frac{p}{E} \times 10^6$

$\frac{D}{h}$

55
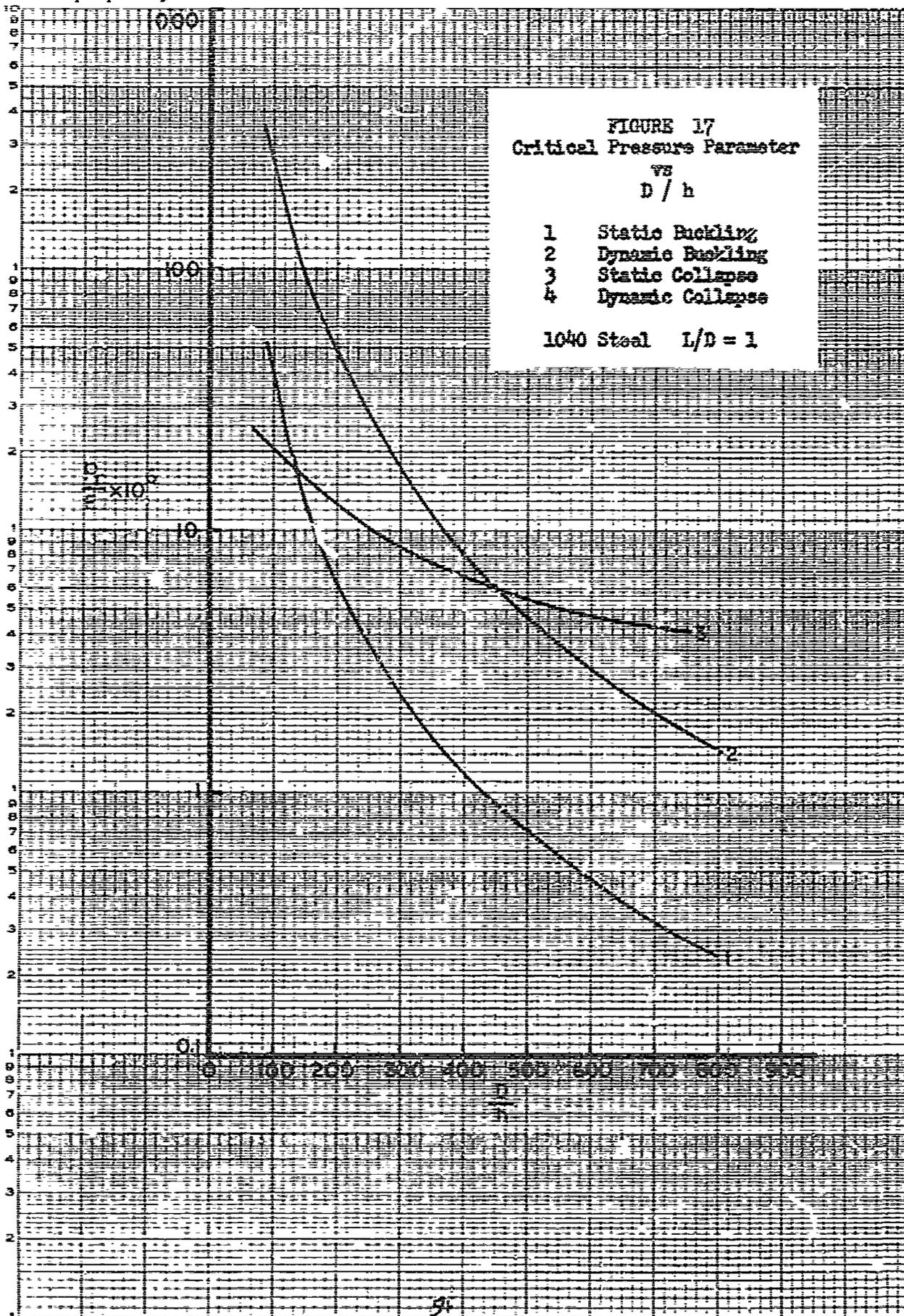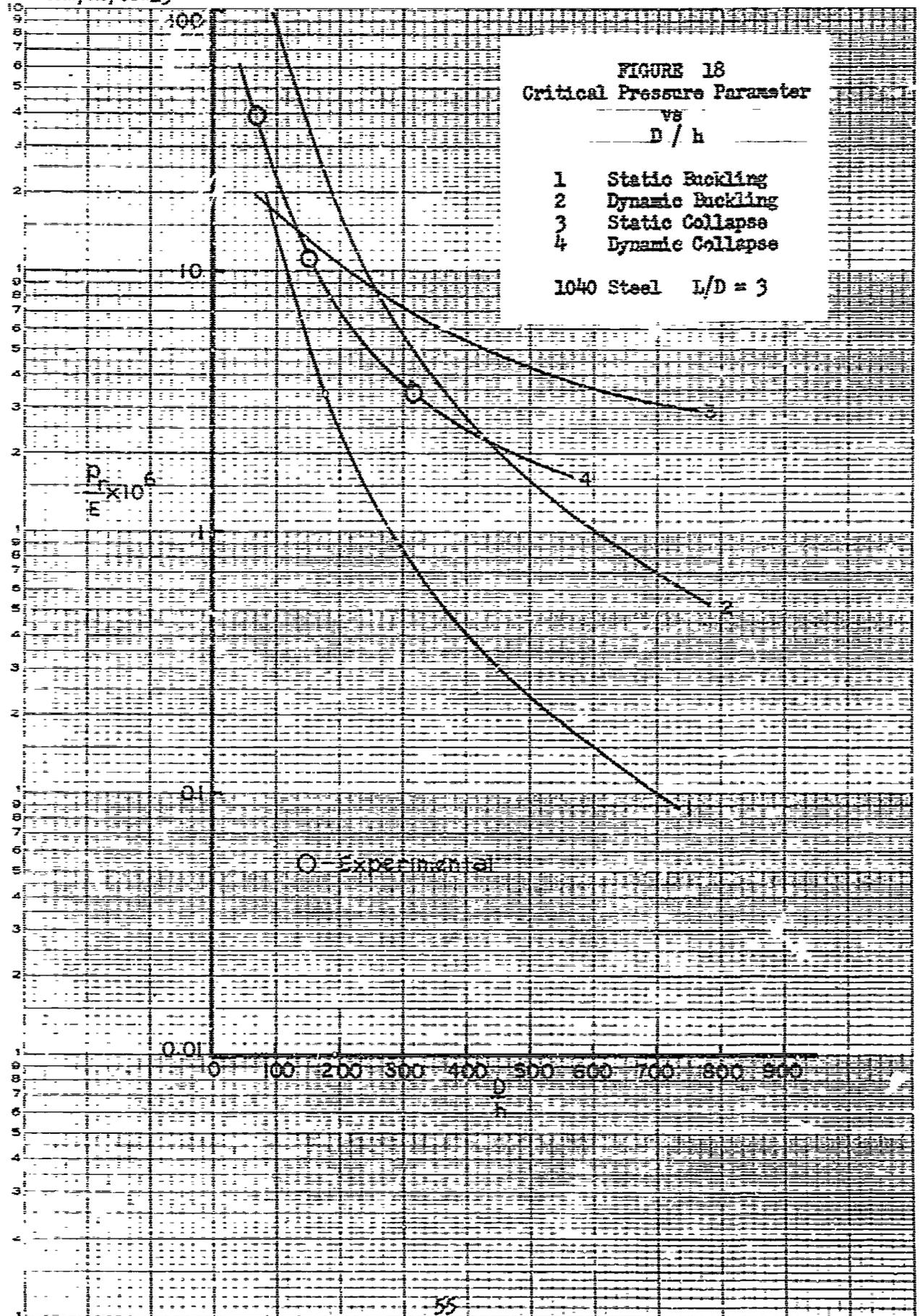
FIGURE 19
Critical Pressure Parameter
vs
D / h

1   Static Buckling
2   Dynamic Buckling
3   Static Collapse
4   Dynamic Collapse

1040 Steel   L/D = 5

FIGURE 20
Critical Pressure Parameter
vs
D / h

1   Static Buckling
2   Dynamic Buckling
3   Static Collapse
4   Dynamic Collapse

6061-T6 Al   L/D = 1

GAW/MC/68-13

FIGURE 21
Critical Pressure Parameter
vs
D / h

1   Static Buckling
2   Dynamic Buckling
3   Static Collapse
4   Dynamic Collapse

6061-T6 Al   L/D = 3

$$\frac{P_r}{E} \times 10^6$$

FIGURE 22
Critical Pressure Parameter
vs
D / h

1 Static Buckling
2 Dynamic Buckling
3 Static Collapse
4 Dynamic Collapse

6061-T6 Al   L/D = 5

71

FIGURE 23
Critical Pressure Parameter
vs
D / h

1   Static Buckling
2   Dynamic Buckling
3   Static Collapse
4   Dynamic Collapse

5052-H38 Al   L/D = 1

GAW/MC/68-13

FIGURE 24
Critical Pressure Parameter
vs
D / h

1   Static Buckling
2   Dynamic Buckling
3   Static Collapse
4   Dynamic Collapse

5052-H38 Al   L/D = 3

61

FIGURE 25
Critical Pressure Parameter
vs
D / h

1   Static Buckling
2   Dynamic Buckling
3   Static Collapse
4   Dynamic Collapse

5052-H38 Al   L/D = 5

FIGURE 26
Critical Pressure Parameter
vs
D / h

1   Static Buckling
2   Dynamic Buckling
3   Static Collapse
4   Dynamic Collapse

1100-0 Al   L/D = 1

FIGURE 27
Critical Pressure Parameter
vs
D / h

1   Static Buckling
2   Dynamic Buckling
3   Static Collapse
4   Dynamic Collapse

1100-0 Al   L/D = 3
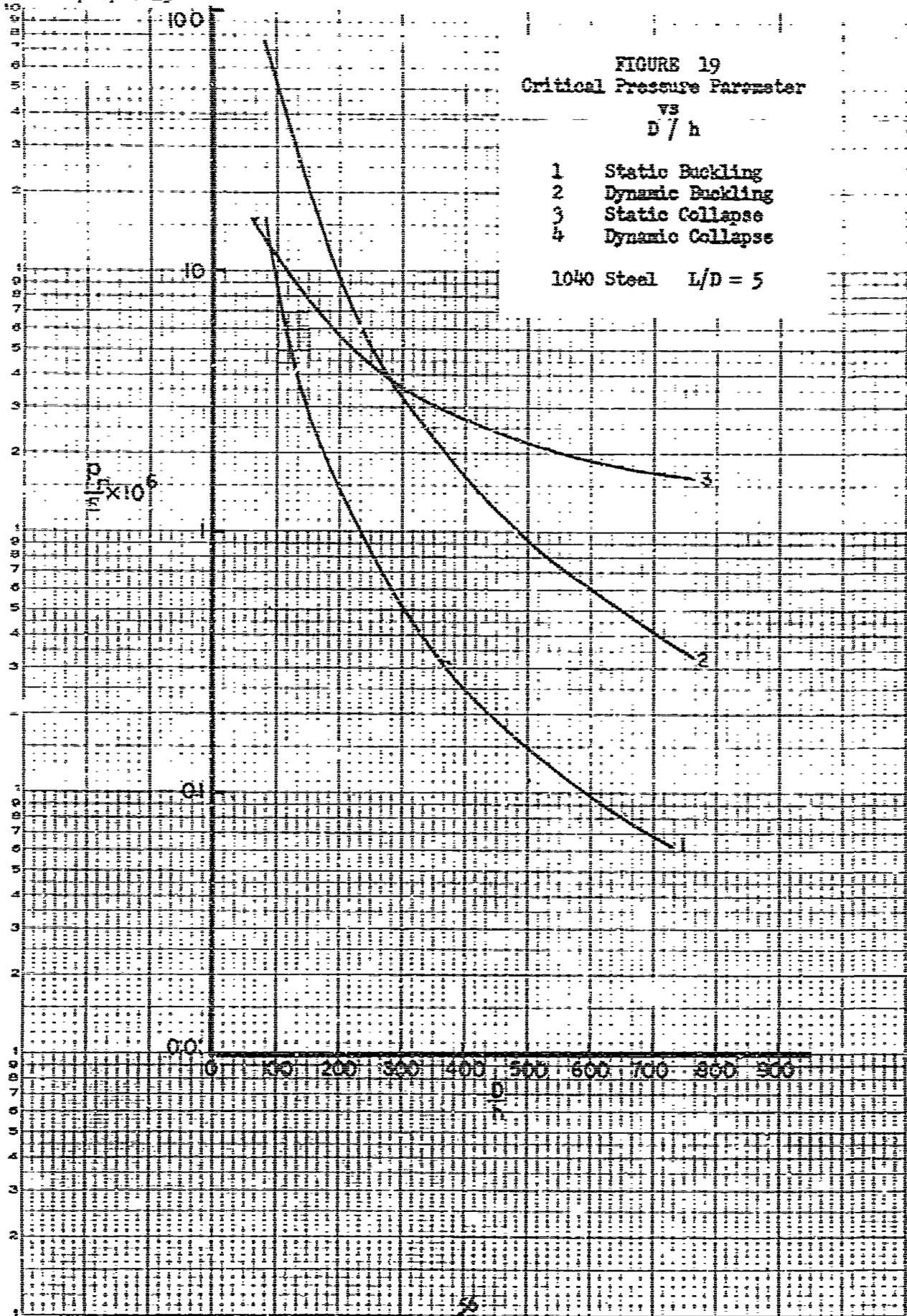
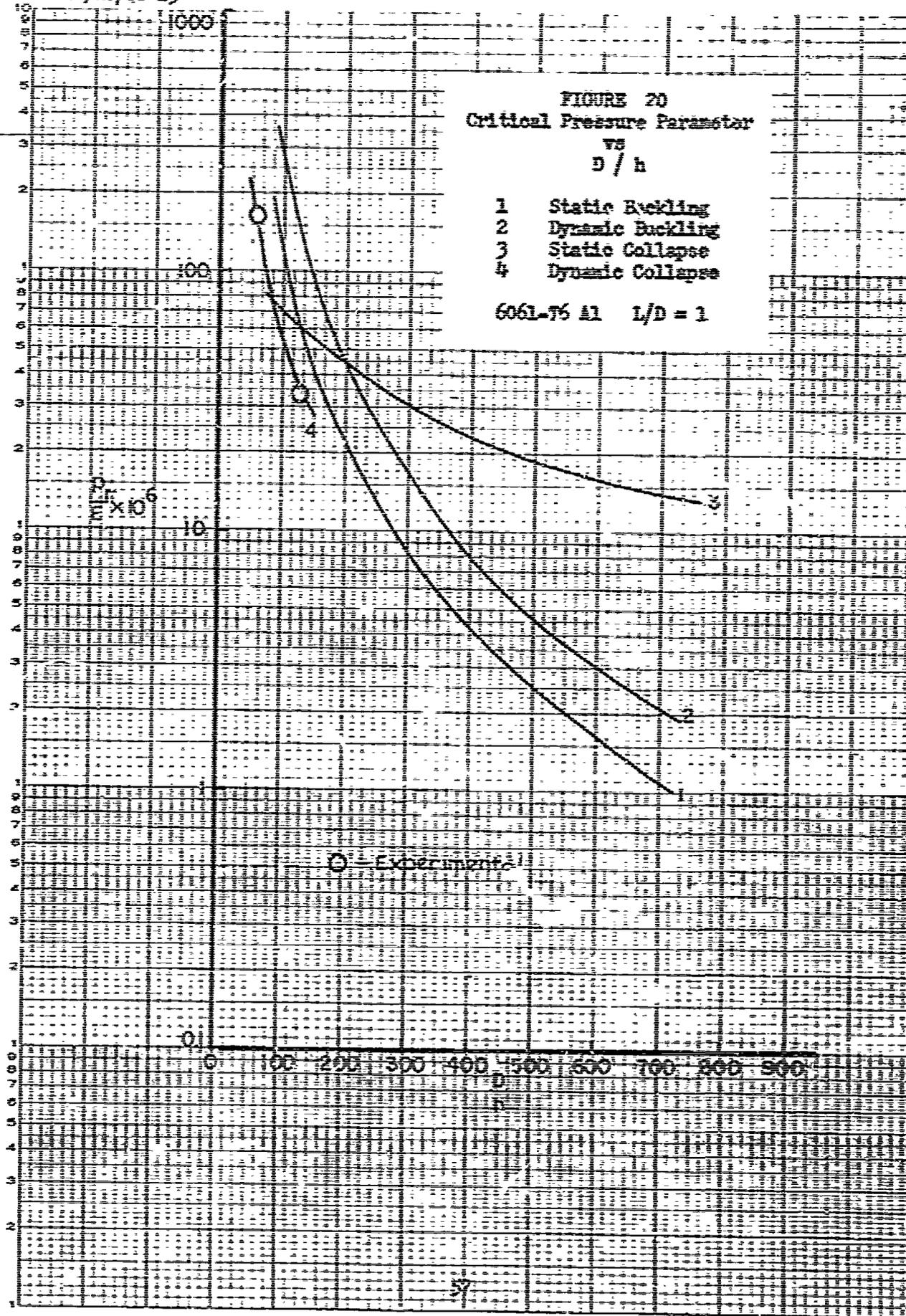FIGURE 28
Critical Pressure Parameter
vs
D / h

1   Static Buckling
2   Dynamic Buckling
3   Static Collapse
4   Dynamic Collapse

1100-0 Al   L/D = 5
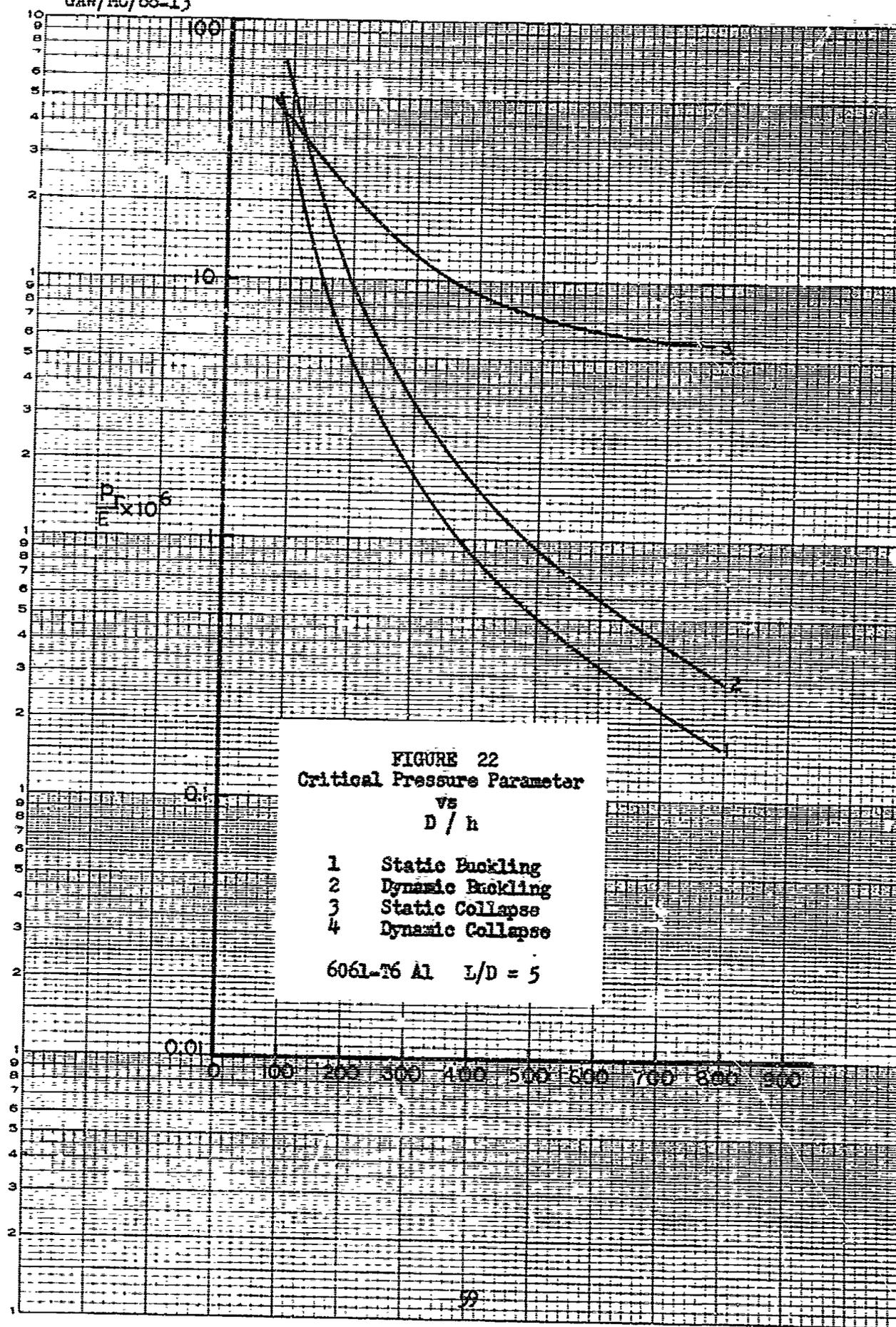
65

VI. Conclusions

The conclusions reached in this report are:

1. The D/h ratio is the dominant shell parameter in determining the failure mode of side-on air blast loaded cylinders.

2. For D/h ratios below 300, the dynamic buckling theory can approximately predict hinge collapse and combination failures.

3. For D/h ratios of 0 to 110, hinge collapse patterns should predominate, 110 to 450 the combination pattern should predominate, and 450 up the wave buckling pattern should predominate.

4. Solution to the dynamic hinge collapse equations cannot be obtained using large values of the pressure decay parameter.

VII. Recommendations

1. It is recommended that numerical integration of equation (91) be attemped using decay parameter (Γ) values between 0.1 and 2.5.

2. It is recommended that a series of experiments be conducted to prove or disprove the limiting value of $D/h = 450$. This might be done with the knowledge that the dynamic collapse curves probably lie below the static collapse curves of Figures 17-28.

3. It is recommended that the solution to the equations in Appendix B be attempted. Their solution would yield a least upper bound to the hinge collapse case.

Bibliography

1. Almroth, B. O. "Buckling of a Cylindrical Shell Subjected to Nonuniform External Pressure." *Journal of Applied Mechanics*, 675-682 (December 1962).

2. Anderson, D. L., Lindberg, H. E., Firth, R. D., and Parker, L. V. *Response of Reentry Vehicle-Type Shells to Blast Loads*. Lockheed Missiles and Space Company, 1965. AD477394.

3. Anderson, J. P. and Woodward, J. H. *The Collapse-Hinge Failure of Blast Loaded Cylinders*. AMC Kaman Nuclear, Colorado Springs, Colorado, 1967, 67-27.

4. ————. *Static Collapse-Hinge Buckling of Cylindrical Shells*. ANC 68-40 Kaman Nuclear, Colorado Springs, Colorado, 1968.

5. Batdorf, S. B. *A Simplified Method of Elastic-Stability Analysis for Thin Cylindrical Shells*. NACA Report No.874, 1947.

6. Brazier, L. G. "On the Flexure of Thin Cylindrical Shells and Other Thin Sections." *Proceedings of The Royal Society*, London, Series A, Vol 116, 104-114 (May 1927).

7. Brush, D. O. and Field, F. A. "Buckling of a Cylindrical Shell Under a Circumferential Band Load." *Journal of the Aerospace Sciences*, 26, 825-830 (1959).

8. Goodier, J. N. and McIvor, I. K. "The Elastic Cylindrical Shell Under Nearly Uniform Radial Impulse." *Journal of Applied Mechanics*, 31, 259-266 (June 1964).

9. Goodman, H. J. *Compiled Free-Air Blast Data on Bare Spherical Pentolite*. U. S. Army BRL Report No. 1092, 1960.

10. Greenspon, J. E. *Post Failure Deflections of Cylindrical Shells Under Dynamic Lateral Loads*. J. G. Engineering Research Associates Tech. Report No. 5, 1954.

11. ————. *Collapse, Buckling, and Post Failure Behavior of Cylindrical Shells Under Elevated Temperature and Dynamic Loads*. J. G. Engineering Research Associates Tech. Report No. 6, 1964.

12. Henrici, P. *Discrete Variable Methods in Ordinary Differential Equations*. New York: John Wiley and Sons, 1962.

13. Schuman, W. J. *A Failure Criterion For Blast Loaded Cylindrical Shells*. U. S. Army BRL Report No. 1292, 1965.

14. Timoshenko, S. Theory of Elastic Stability (First Edition).
     New York: McGraw Hill Book Company, 1936.

15. Timoshenko, D. and Woinowsky-Kriege, S. Theory of Plates
     and Shells. New York: McGraw Hill Book Company, 1959.

Appendix A

The input data necessary for operation of this program is:

1. L/D, D/h, shell diameter (DIA) according to format statement 100

2. PI and Poisson's ratio (NU) according to format statement 105

3. pressure parameter (PRED), mass density per unit volume (RHO), and Young's modulen (EYO) according to format statement 110.

The output of this program is:

1. Brazier's moment (MCB), D/h, and L/D ratios according to format statement 115

2. time (x), maximum moment (MMAX), Brazier's moment (MCB), and pressure decay parameter (ALPHA) according to format statement 120

3. coefficient A_1 (t) (Y(2), pressure parameter (PRED), Young's modulus (EYO), and maximum moment (MMAX) according to format statement 125.

PROGRAM VARIABLES

LD	L/D ratio
DH	D/h ratio
DIA	shell diameter
PI	pi, 3.14159
NU	Poisson's ratio
EYO	Young's modulus
RHO	mass density per unit length
PRED	PRESSURE PARAMETER, $p_r \times 10^6 / E$
C1 to C11	coefficients of equation (91)
Y(2)	Coefficient, $A_1(t)$
MCB	Brazier's collapse moment, equation (97)
X	time, t
ALPHA	decay parameter, p_r / I_r

```
C
C                    DYNAMIC ANALYSIS PROGRAM
C
      COMMON/CMN1/M,N,H,X,Y(2),F(2),OLD(2),PHI(2),OLDY(2)
      REAL LD,LD2,LD4,LD6,LD8,NU,MCB,XMAX
C
C                    PROGRAM PROPER
C
      DIMENSION B(1)
      READ   (5,105)  PI, NU
5     READ   (5,100)  LD,DIA,ALPHA,DH,H,XMAX
      READ   (5,110)  PRED, RHO, EYO
      WRITE  (6,105)  PI,NU
      WRITE  (6,100)  LD,DIA,ALPHA,DH,H,XMAX
      DO 12 I = 1,7,1
      PI2 = PI*PI
      PI4 = PI2*PI2
      PI6 = PI4*PI2
      PI8 = PI4*PI4
      DH2 = DH*DH
      DH4 = DH2*DH2
      DIA2 = DIA*DIA
      ZUL = 1. - NU*NU
      ZUL2 = ZUL*ZUL
      LD2 = LD*LD
      LD4 = LD2*LD2
      LD6 = LD4*LD2
      LD8 = LD4*LD4
      C1 = 32.*LD8
      C2 = C1*DIA2
      C3 = 5.*DH4*ZUL2*PI8
      C4 = (64.4*DIA*DH)/1.0E+12
      C6 = (128.8*PI4)/(LD8*DIA2*1.0E+06)
      C8 = 1.15*ZUL*PI4*DH2
      C9 = LD4*DIA2
      C10 = (0.15625*PI8*DH4*ZUL2)/LD8
      C11 = (6.0*PI2*LD2)/DIA2
      AB = EYO/RHO
      C7 = C6*AB
      MCB = ((0.4935)/(DH2*SQRT(ZUL)))
      WRITE (6,115)  MCB,DH,LD,EYO
      M = 0
      N = 2
10    Y(1) = 0.
      Y(2) = 0.
      X = 0.
      C5 = C4*AB*PRED
3     CALL RUNGA
      IF (M) 1,2,1
1     BETA = -ALPHA*X
      F(2) = (C1/(C2 +C3*(Y(1)**2)))*((C5*EXP(BETA)) + (C7*(C8*(Y(1)**2
     1) - C9)*Y(1)) - (C10*Y(1)*(Y(2)**2)) + C7*C11*(Y(1)**3))
      F(1) = Y(2)
```

72

```
          GO TO 3
  2       B(1) = Y(1)
          Y(1) = Y(1)/DIA
          MMAX = ((PI*DI2)/(LD**2))*((.25/DH)-(((.375*PI4*DH*ZUL)/(LD**4))
         1*(Y(1)**2)))*Y(1)
          IF (ABS(MMAX).GT.MCB) GO TO 26
          Y(1) = B(1)
          IF (X-XMAX) 3,25,25
  25      PRED = PRED + 10.
          WRITE (6,125) Y(1),PRED,X,MMAX,ALPHA
          GO TO 10
  26      Y(1) = B(1)
          WRITE (6,125) Y(1),PRED,X,MMAX,ALPHA
          DH = DH + 100.
          PRED = 18.
  12      CONTINUE
          GO TO 5
  C
  C                      FORMAT STATEMENTS
  C
  100     FORMAT  (6F12.4)
  105     FORMAT  (2E15.7)
  110     FORMAT  (3E15.7)
  115     FORMAT (1H0,10X,5HMCB =,F16.8,5X,4HDH =,E11.3,5X,4HLD =,E11.3,5X,
         15HEYO =,E11.3)
  125     FORMAT    (5 X,7HY(1) = ,E16.8,5X,6HPRED =,E12.4,5X,6HTIME =,E16.8
         1,5X,7HMMAX = ,E12.4,5X,7HALPHA =,E12.4)
          END
          SUBROUTINE RUNGA
          COMMON/CMN1/M,N,H,X,Y(2),F(2),OLD(2),PHI(2),OLDY(2)
          M=M+1
          GO TO (15,11,12,13,14),M
  15      RETURN
  11      DO 20 J=1,N
  20      OLDY(J)=Y(J)
          DO 21 J=1,N
  21      PHI(J) = F(J)
          DO 22 J=1,N
  22      Y(J)=OLDY(J)+.5*H*F(J)
          X=X+.5*H
          RETURN
  12      DO 23 J=1,N
  23      PHI(J)=PHI(J)+2.*F(J)
          DO 24 J = 1,N
  24      Y(J)=OLDY(J)+.5*H*F(J)
          RETURN
  13      DO 25 J=1,N
  25      PHI(J)=PHI(J)+2.*F(J)
          DO 26 J=1,N
  26      Y(J)=OLDY(J)+H*F(J)
          X=X+.5*H
          RETURN
```

73

```
14    DO 27 J=1,N
27    PHI(J)=PHI(J)+F(J)
      DO 28 J=1,N
28    Y(J)=OLDY(J)+PHI(J)*H/6.
      M=0
      RETURN
      END
```

Appendix B

The governing differential equations, including non-linear change-of-curvature terms are given by Timoshenko (Ref 4:15) as

$$a \frac{\partial N_x}{\partial x} + \frac{\partial N_{\theta x}}{\partial \theta} - a N_{x\theta} V_{xx} - N_\theta (V_{\theta x} - W_x) = 0 \qquad (B-1)$$

$$\frac{\partial N_\theta}{\partial \theta} + a \frac{\partial N_{x\theta}}{\partial \theta} + \frac{\partial M_{\theta x}}{\partial \theta} - \frac{1}{a} \frac{\partial M_\theta}{\partial \theta} + a N_x V_{xx} + N_{\theta x}(V_{x\theta} - W_x) = 0 \qquad (B-2)$$

$$N_\theta + \frac{\partial^2 M_{\theta x}}{\partial x \partial \theta} + a \frac{\partial^2 M_x}{\partial x^2} - \frac{\partial^2 M_{x\theta}}{\partial \theta \partial x} + \frac{1}{a} \frac{\partial^2 M_\theta}{\partial \theta^2} + N_\theta (V_\theta - W_{\theta\theta}) \frac{1}{a}$$

$$+ a N_x W_{xx} + 2 N_{x\theta}(V_x - W_{x\theta}) + p a = 0 \qquad (B-3)$$

where U, V, W are shown in Figure 1 and N_x, $N_{x\theta}$, N_θ, M_x, $M_{x\theta}$ & M_θ are shown in Figure B-1. The relation between the forces and displacements and moments and displacements are

$$N_x = \frac{Eh}{1-\nu^2} \left[U_x + \frac{\nu}{2} (V_\theta - W) \right] \qquad (B-4)$$

$$N_\theta = \frac{Eh}{1-\nu^2} \left[\frac{1}{a}(V_\theta - W) + \nu U_x \right] \qquad (B-5)$$

$$N_{x\theta} = \frac{Eh}{2(1+\nu)} \left[\frac{1}{a} U_\theta + U_x \right] \qquad (B-6)$$

$$M_x = -D \left[W_{xx} + \frac{\nu}{a}(V_\theta + W_{\theta\theta}) \right] \qquad (B-7)$$

$$M_\theta = -D \left[\frac{1}{a^2}(V_\theta + W_{\theta\theta}) + \nu W_{xx} \right] \qquad (B-8)$$

$$M_{x\theta} = -M_{\theta x} = D(1-\nu) \left[\frac{1}{a}(V_x + W_{x\theta}) \right] \qquad (B-9)$$

where

$$D = \frac{Eh^3}{12(1-\nu^2)} \qquad (B-10)$$

Defined non-dimensional coordinates as

$$u = \frac{U}{a} \tag{B-11}$$

$$v = \frac{V}{a} \tag{B-12}$$

$$w = \frac{W}{a} \tag{B-13}$$

$$\xi = \frac{x}{a} \tag{B-14}$$

equations (B-1) to (B-3) can be written as

$$u_{\xi\xi} + \frac{1-\nu}{2} u_{\theta\theta} + \frac{1+\nu}{2} v_{\xi\theta} - \nu w_{\xi} - (1-\nu^2)\left[\frac{N_{x\theta}}{Eh} v_{\xi\xi} \right.$$
$$\left. + \frac{N_\theta}{Eh}(v_{\xi\theta} - w_\xi) \right] = 0 \tag{B-15}$$

$$\frac{1+\nu}{2} u_{\xi\theta} + \frac{1-\nu}{2} v_{\xi\xi} + v_{\theta\theta} - w_\theta + q\left[w_{\xi\xi\theta} + w_{\theta\theta\theta} + (1-\nu) \right.$$
$$\left. \circ v_{\xi\xi} + v_{\theta\theta} \right] + (1-\nu^2)\left[\frac{N_x}{Eh} v_{\xi\xi} + \frac{N_{x\theta}}{Eh}(v_{\xi\theta} - w_\xi) \right] = 0 \tag{B-16}$$

$$\nu u_\xi + v_\theta - w - q\left[w_{\xi\xi} + 2w_{\xi\xi\theta\theta} + w_{\theta\theta\theta\theta} + (2-\nu)v_{\xi\xi\theta} + v_{\theta\theta\theta} \right]$$
$$+ (1-\nu^2)\left[\frac{N_x}{Eh} w_{\xi\xi} + \frac{2N_{x\theta}}{Eh}(v_\xi + w_{\xi\theta}) \right] + \frac{p\,a}{Eh}(1-\nu^2) = 0 \tag{B-17}$$

where

$$q = \frac{1}{12}\left(\frac{h}{a}\right)^2 \tag{B-18}$$

The method of solution of these equations involves the assumption that the shell is inextensional in the circumferential direction or

$$v_\theta - w = 0 \tag{B-19}$$

and the displacement components can be expressed as

76

$$u = h_1'(\xi)\cos\theta + h_2'(\xi)\cos 2\theta + \cdots \qquad (B\text{-}20)$$

$$v = g_1(\xi)\sin\theta + g_2(\xi)\sin 2\theta + \cdots \qquad (B\text{-}21)$$

$$w = g_1(\xi)\cos\theta + 2g_2(\xi)\cos 2\theta + \cdots \qquad (B\text{-}22)$$

Applying equation (B-19) to the system of equations (B-1) thru (B-3) results in a set of equations that are insensitive to the circumferential extensional mode. In the resulting equations, equation (B-1) remains the same, the linear term in N_θ is eliminated in the second and third equations, and the linear term in $N_{x\theta}$ is eliminated from the resulting expression by use of equation (B-1). These manipulated set of equations may thus be written as

$$a\frac{\partial N_x}{\partial x} + \frac{\partial N_{x\theta}}{\partial\theta} - aN_{x\theta}V_{x\theta} - N_\theta(W_{x\theta} - W) = 0 \qquad (B\text{-}23)$$

$$a\frac{\partial^4 M_{x\theta}}{\partial x\partial\theta^3} + \frac{\partial^2 M_{x\theta}}{\partial x\partial\theta} - \frac{1}{a}\frac{\partial^4 M_\theta}{\partial\theta^4} - \frac{1}{a}\frac{\partial^2 M_\theta}{\partial\theta^2} - a\frac{\partial^4 M_x}{\partial x^2\partial\theta^2}$$

$$- a^2\frac{\partial^2 N_x}{\partial x^2} + \frac{\partial}{\partial\theta}\left[aN_x V_{xx} + N_{x\theta}(V_{x\theta} - W_x)\right]$$

$$+ \frac{\partial}{\partial x}\left[a^2 N_{x\theta}V_{xx} + aN_\theta(V_{x\theta} - W_x)\right] + \frac{\partial^2}{\partial\theta^2}\left[\frac{1}{a}N_\theta(V_\theta + W_{\theta\theta})\right.$$

$$\left. + aN_x W_{xx} + 2N_{x\theta}(V_x + W_{xx})\right] - a\frac{\partial^2 P}{\partial\theta^2} = 0 \qquad (B\text{-}24)$$

Assuming $P(\theta)$ can be expressed as

$$P(\theta) = P_o + P_1\cos\theta + P_2\cos 2\theta + \cdots \qquad (B\text{-}25)$$

and using equations (B-20) to (B-21), the governing set of equations become

77

$$h_1'''(\xi)\cos\theta + \frac{1-\nu}{2}\left\{h_1'(\xi)\left[g_1''(\xi)\sin\theta - 1\right]\cos\theta + g_1'(\xi)\cos\theta\right.$$

$$\left. - g_1'(\xi)g_1''(\xi)\sin^2\theta\right\} = 0 \qquad \text{(B-26)}$$

$$h_1''(\xi)g_1''(\xi)\left[2\cos^2\theta + \cos 2\theta\right] - \frac{1}{12}\left(\frac{h}{a}\right)^2 g_1''''\cos\theta$$

$$-h_1''''(\xi)\cos\theta + \frac{1-\nu}{2}\left\{g_1''(\xi)\left[g_1''(\xi) - h_1''(\xi)\right]\right.$$

$$\left. + g_1'''(\xi)\left[g_1'(\xi) - h_1'(\xi)\right]\right\}\sin^2\theta = -\frac{(1-\nu^2)R\cos\theta}{E\left(\frac{h}{a}\right)} \qquad \text{(B-27)}$$

$$h_2'''\cos 2\theta + (1-\nu)\left[g_2'(\xi) - 2h_2'(\xi)\right]\cos 2\theta$$

$$-(1-\nu)\left[g_2'(\xi) - h_2'(\xi)\right]\bar{g}_2''(\xi)\sin^2 2\theta = 0 \qquad \text{(B-28)}$$

$$2h_2''(\xi)g_1''(\xi)\left[8\cos^2 2\theta + \cos 4\theta\right] - \frac{2}{3}\left(\frac{h}{a}\right)^2 g_2''''(\xi)\cos 2\theta$$

$$-h_2''''(\xi)\cos 2\theta + \frac{(1-\nu)}{2}\left\{g_2''(\xi)\left[g_2''(\xi) - 2h_2''(\xi)\right]\right.$$

$$\left. + g_2'''(\xi)\left[g_1'(\xi) - 2h_2'(\xi)\right]\right\}\sin^2 2\theta$$

$$= -\frac{4(1-\nu^2)P_2\cos 2\theta}{E\left(\frac{h}{a}\right)} \qquad \text{(B-29)}$$

Solution of equations (B-26) thru (B-29) is not easily accomplished analytically. Since there is no standard procedure to solve these

coupled non-linear differential equations by numerical intergration, their solution is not attempted in this paper.

Note that if the same simplifing assumptions used in (Ref 4:19) are used on equation (B-26) thru (B-29), the resulting expressions are the same as found on page 19 of (Ref 4).
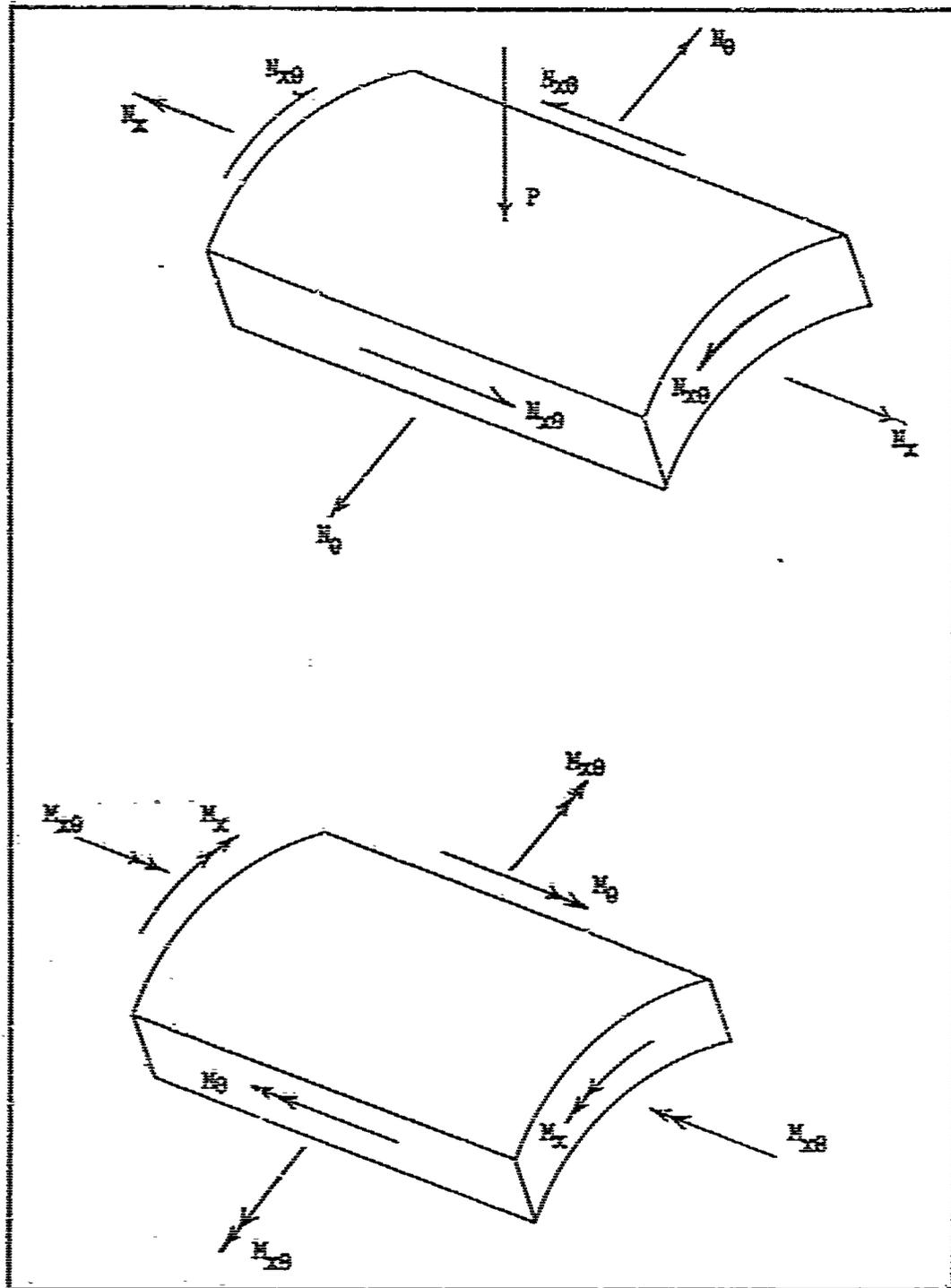
FIGURE B-1

Cylinder Shell Element Stress Resultants
(Ref 4:47)

Appendix C

The input data necessary for operation of this program is:

1. Young's modulus (EYO) and mass density (RHO) according to format statement 100

2. setting the initial value of shell radius, A

3. setting the initial value of L/D ratio, LD

4. setting the initial D/h ratio

The output of this program is:

1. Young's modulus (EYO) and mass density per unit volume (RHO) according to format statement 105

2. the asymptotic values of pressure and impulse (PE and IE), radius to length ratio (AL), diameter to thickness ratio (HA), and pressure parameter (PRED) according to format statement 115

3. the pressure (P) and impulse (IMP) for iso-damage curves of the elastic modulus buckling theory according to the format statement 120

PROGRAM VARIABLES

P	pressure, P_r
PE	asmypototic pressure
PRED	pressure parameter PE x 10^6/ E
IMP	impulse, I_r
IE	asymptotic impulse
YO	Young's modulus, E
RHO	mass density per unit volume
A	shell radius
LD	L/D ratio
AL	radius to length ratio
HA	a/h ratio

```
$IBJOB          MAP
$IBFTC MAIN
      REAL IE   ,LD
      REAL IMP
  5   READ (5,100) EYO,RHO
      WRITE (6,105) EYO,RHO
      A = 1.5
      LD = 1.
      BETA = (RHO*EYO)/(12.*32.2)
      DO 11  J = 1,3,1
      AL = .5/LD
      HA = 50.
      DO 10 K = 1, ,1
      PE = (0.92*EYO*AL)/(HA**2.5)
      IE = (5.*A*SQRT(BETA)*1000.)/(HA**2)
      PRED = (PE*1.0E+6)/EYO
      WRITE (6,115) AL,HA,PE,IE,PRED
      P = PE + 5.
      DO 12 I=1,10,1
      IMP = ((IE*PE)/(P-PE)) + IE
      WRITE (6,120) P,IMP
      P = P + 10.
 12   CONTINUE
      HA = HA + 50.
 10   CONTINUE
      LD = LD + 2.
 11   CONTINUE
      GO TO 5
 100  FORMAT (E16.8,E12.4)
 105  FORMAT (1H0,15X,5HEYO =,E16.8,10X,5HRHO =,E12.4)
 115  FORMAT (1H0,5X,4HAL =,E10.2,5X,4HHA =,E12.4,5X,4HPE =,E16.8,5X,
     1 4HIE =,E16.8,5X,6HPRED =,E16.8)
 120  FORMAT(1H0,3HP =,E16.8,5X,5HIMP =,E16.8)
      END
```

TABLE C - 1
STATIC BUCKLING PRED VALUES

MATERIAL \ b/h	L/b	100	200	300	400	500	600	700
1040 STEEL	1	36.80	6.21	2.53	1.13	0.73	0.46	0.31
6061-T6 AL		128.0	21.6	8.80	3.92	2.60	1.60	1.08
5052-H38 AL		116.2	15.62	7.99	3.56	2.36	1.45	0.98
1100-O AL		16.00	2.70	1.10	0.49	0.33	0.20	0.14
1040 STEEL	3	13.89	2.36	0.99	0.39	0.24	0.15	0.10
6061-T6 AL		48.00	8.20	3.44	1.36	0.84	0.52	0.35
5052-H38 AL		43.56	7.44	3.12	1.23	0.76	0.47	0.32
1100-O AL		6.0	1.03	0.43	0.17	0.11	0.07	0.04
1040 STEEL	5	8.97	1.38	0.62	0.24	0.15	0.09	0.07
6061-T6 AL		31.20	4.80	2.16	0.82	0.52	0.32	0.23
5052-H38 AL		28.31	4.36	1.96	0.74	0.47	0.29	0.21
1100-O AL		3.90	0.60	0.27	0.10	0.07	0.04	0.03

TABLE C - 2
DYNAMIC BUCKLING PRED VALUES

MATERIAL	D/h	100	200	300	400	500	600	700	L/D
1040 STEEL		260.2	46.10	16.70	8.10	4.70	3.00	2.00	1
6061-T6 AL		260.2	46.10	16.70	8.10	4.70	3.00	2.00	
5052-H38 AL		260.2	46.10	16.70	8.10	4.70	3.00	2.00	
1100-0 AL		250.2	46.10	16.70	8.10	4.70	3.00	2.00	
1040 STEEL		86.70	15.30	5.60	2.70	1.60	1.00	0.70	3
6061-T6 AL		86.70	15.30	5.60	2.70	1.60	1.00	0.70	
5052-H38 AL		86.70	15.30	5.60	2.70	1.60	1.00	0.70	
1100-0 AL		86.70	15.30	5.60	2.70	1.60	1.00	0.70	
1040 STEEL		52.00	9.20	3.30	1.60	0.90	0.60	0.40	5
6061-T6 AL		52.00	9.20	3.30	1.60	0.90	0.60	0.40	
5052-H38 AL		52.00	9.20	3.30	1.60	0.90	0.60	0.40	
1100-0 AL		52.00	9.20	3.30	1.0	0.90	0.60	0.40	

TABLE C - 3
STATIC COLLAPSE PRED VALUES

MATERIAL \ D/t	100	200	300	400	500	600	700	L/b
1040 STEEL	19.95	11.61	8.97	6.44	5.75	4.72	4.03	1
6061-T6 AL	68.00	40.40	31.20	22.40	20.00	16.40	14.00	
5052-H38 AL	61.71	36.66	28.31	20.33	18.15	14.88	12.71	
1100-O AL	8.50	5.05	3.90	2.80	2.50	2.05	1.75	
1040 STEEL	17.25	10.47	7.02	5.29	4.72	3.68	3.22	3
6061-T6 AL	60.00	36.40	24.40	18.40	16.40	12.80	11.20	
5052-H38 AL	54.45	33.03	22.14	16.70	14.88	11.62	10.16	
1100-O AL	7.50	4.55	3.05	2.30	2.05	1.60	1.40	
1040 STEEL	11.50	5.75	3.68	2.30	2.19	2.07	1.73	5
6061-T6 AL	40.00	20.00	12.80	8.00	7.60	7.20	6.00	
5052-H38 AL	36.30	18.15	11.62	7.26	6.90	6.53	5.45	
1100-O AL	5.00	2.50	1.60	1.00	0.95	0.90	0.75	

TABLE C - 4
DYNAMIC COLLAPSE PRED VALUES

(Values from data of Reference 13, blanks indicate no data available)

MATERIAL \ D/h	100	200	300	400	500	600	700	L/D
1040 Steel								
6061-T6 AL	5.2							1
5052-H38 A L								
1100-0 AL								
1040 Steel	22.0	7.0	3.7	2.45	1.9			
6061-T6 AL	50.0	13.5						3
5052-H38 AL	21.0	8.5	4.3	1.65	1.1			
1100-0 AL		8.0	4.0	2.4	1.6	1.1		
1040 Steel								
6061-T6 AL								5
5052-H38 AL								
1100-0 AL								

TABLE C-5

ASYMPTOTIC PRESSURES AND IMPULSES (DYNAMIC BUCKLING-ELASTIC MODEL)

$1/D$	MATERIAL	D/h	100		200		300		400		500		600		700	
			P_E	I_E	P_E	I_E	P_E	I_E	P_E	I_E	P_E	I_E	P_E	I_E	P_E	I_E
1	1040 STEEL		780.6	424.6	138.	106.1	50.1	47.2	24.4	26.5	14.0	17.0	8.85	11.8	6.02	8.67
	6061-T6 AL		260.2	151.1	46.0	37.8	16.7	16.8	8.13	9.44	4.65	6.04	2.95	4.20	2.01	3.08
	5052-H38 AL		265.4	151.8	46.9	37.8	17.0	16.9	8.39	9.49	4.75	6.07	3.01	4.22	2.05	3.10
	1100-0 AL		260.2	151.1	46.0	37.8	16.7	16.8	8.13	9.44	4.65	6.04	2.95	4.20	2.01	3.08
3	1040 STEEL		260.2	424.6	46.0	106.1	16.7	47.2	8.13	26.5	4.65	17.0	2.95	11.8	2.01	8.67
	6061-T6 AL		86.7	151.1	15.3	37.8	5.56	16.8	2.71	9.44	1.55	6.04	0.98	4.20	0.67	3.08
	5052-H38 AL		88.5	151.8	15.6	37.9	5.68	16.9	2.76	9.49	1.58	6.07	1.00	4.22	0.68	3.10
	1100-0 AL		86.7	151.1	15.3	37.8	5.56	16.8	2.71	9.44	1.55	6.04	0.98	4.20	0.67	3.08
5	1040 STEEL		156.1	424.6	27.6	106.1	10.0	47.2	4.88	26.5	2.79	17.0	1.77	11.8	1.20	8.67
	6061-T6 AL		52.0	151.1	9.20	37.8	3.34	16.8	1.63	9.44	0.93	6.04	0.59	4.20	0.40	3.08
	5052-H38 AL		53.1	151.8	9.38	37.9	3.41	16.9	1.66	9.49	0.95	6.07	0.60	4.22	0.41	3.10
	1100-0 AL		52.0	151.1	9.20	37.8	3.34	16.8	1.63	9.44	0.93	6.04	0.59	4.20	0.40	3.08

TABLE C - 6
MATERIAL PROPERTIES

MATERIAL / MATERIAL PROPERTY	E lbf/in^2	ρ lbm/in^2	K *	σ_y lbf/in^2
1040 STEEL	30×10^6	.258	——	34,500
6061-T6 ALUMINUM	10.0×10^6	.098	30	40,000
5052-H38 ALUMINUM	10.2×10^6	.097	32	37,000
1100-0 ALUMINUM	10.0×10^6	.098	34	5,000

* Ref (2 : 217)

Appendix D

The following table of blast parameters is for the shells appearing in this section.

TABLE D – 1
BLAST PARAMETERS

BLAST PARAM. FIGURE	P_r psi	I_r psi - msec
D-1 , IT 5	8.5	18.0
D-2 , IT 10	6.5	16.0
D-3 , IT 15	5.5	13.0
D-4 , IT 1	20.0	6.85
D-5 , IT 4	8.5	4.1
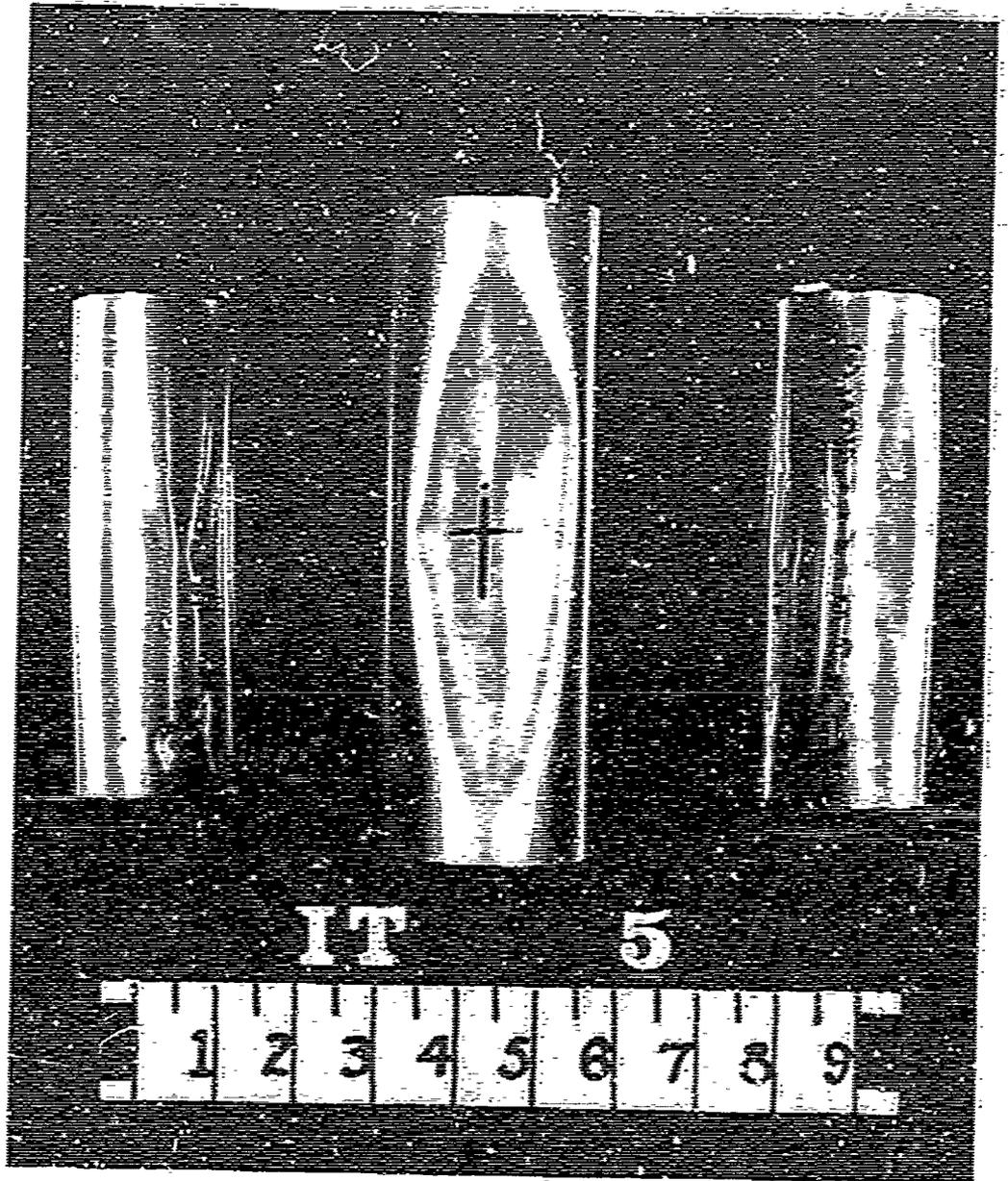
FIGURE D-1
Collapse, 1100-Al
D = 2.75 in., L/D = 3.33, D/h = 275
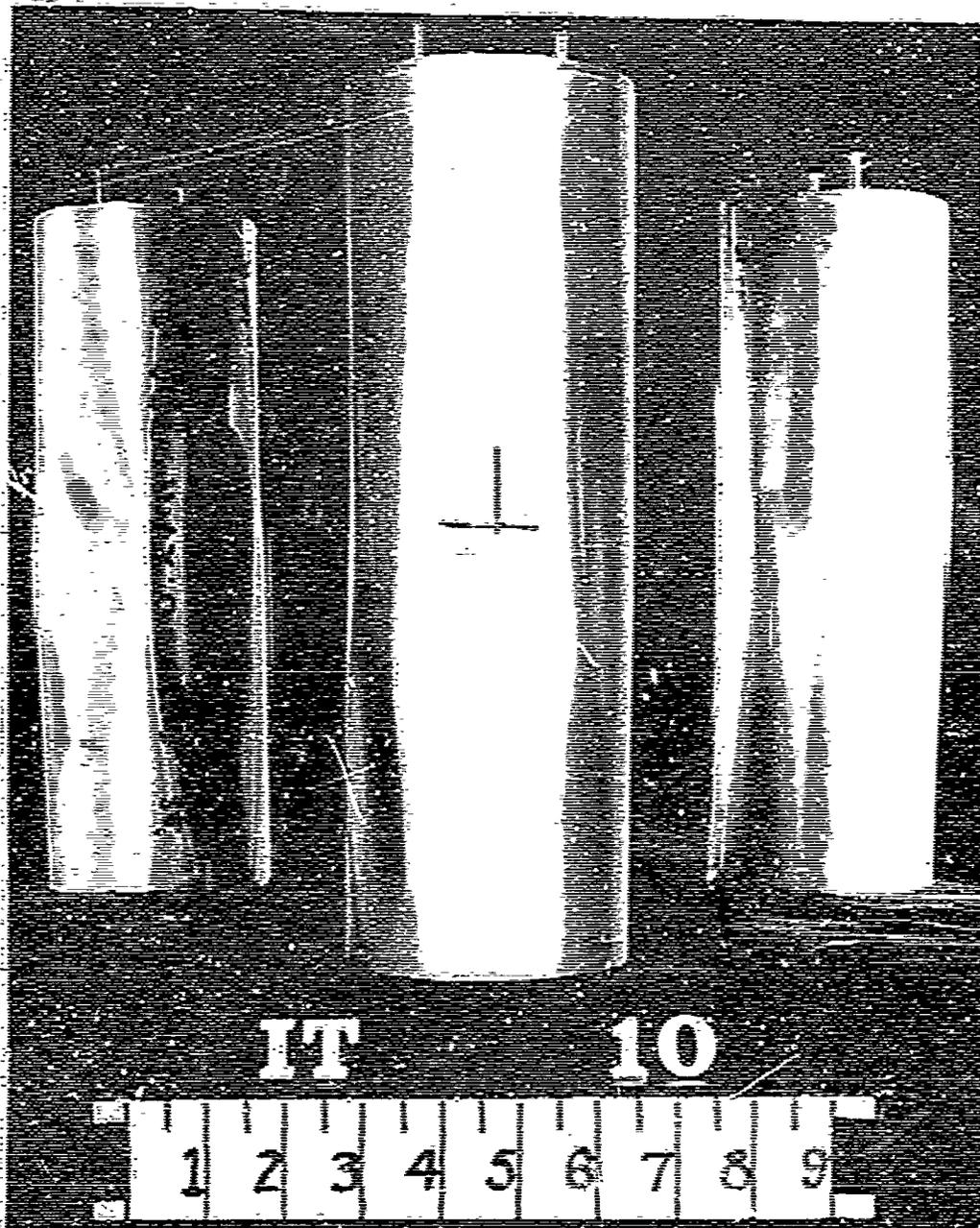
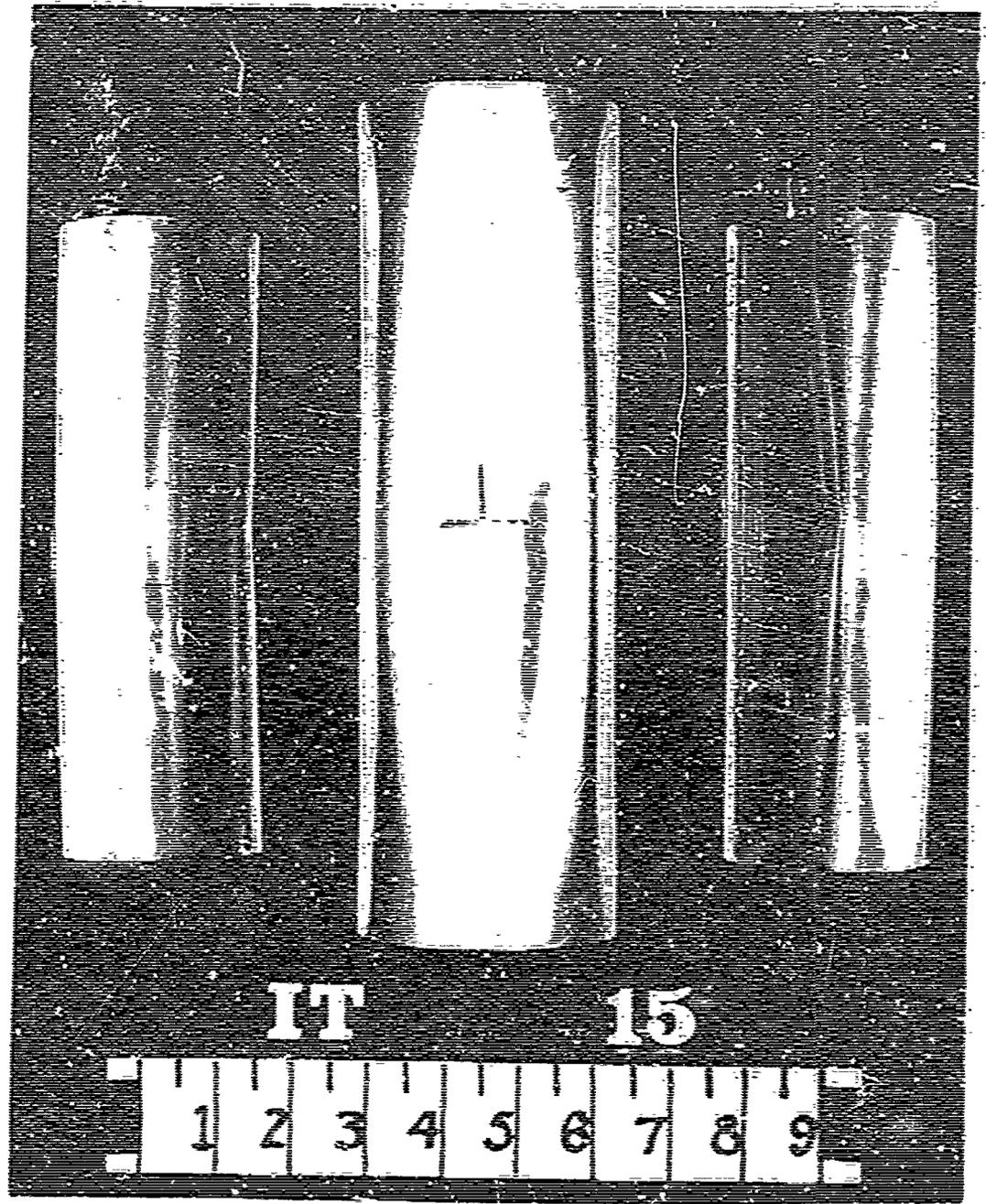FIGURE D-2
Combination, 1100-Al
D = 3.75 in., L/D = 3.33, D/h = 375
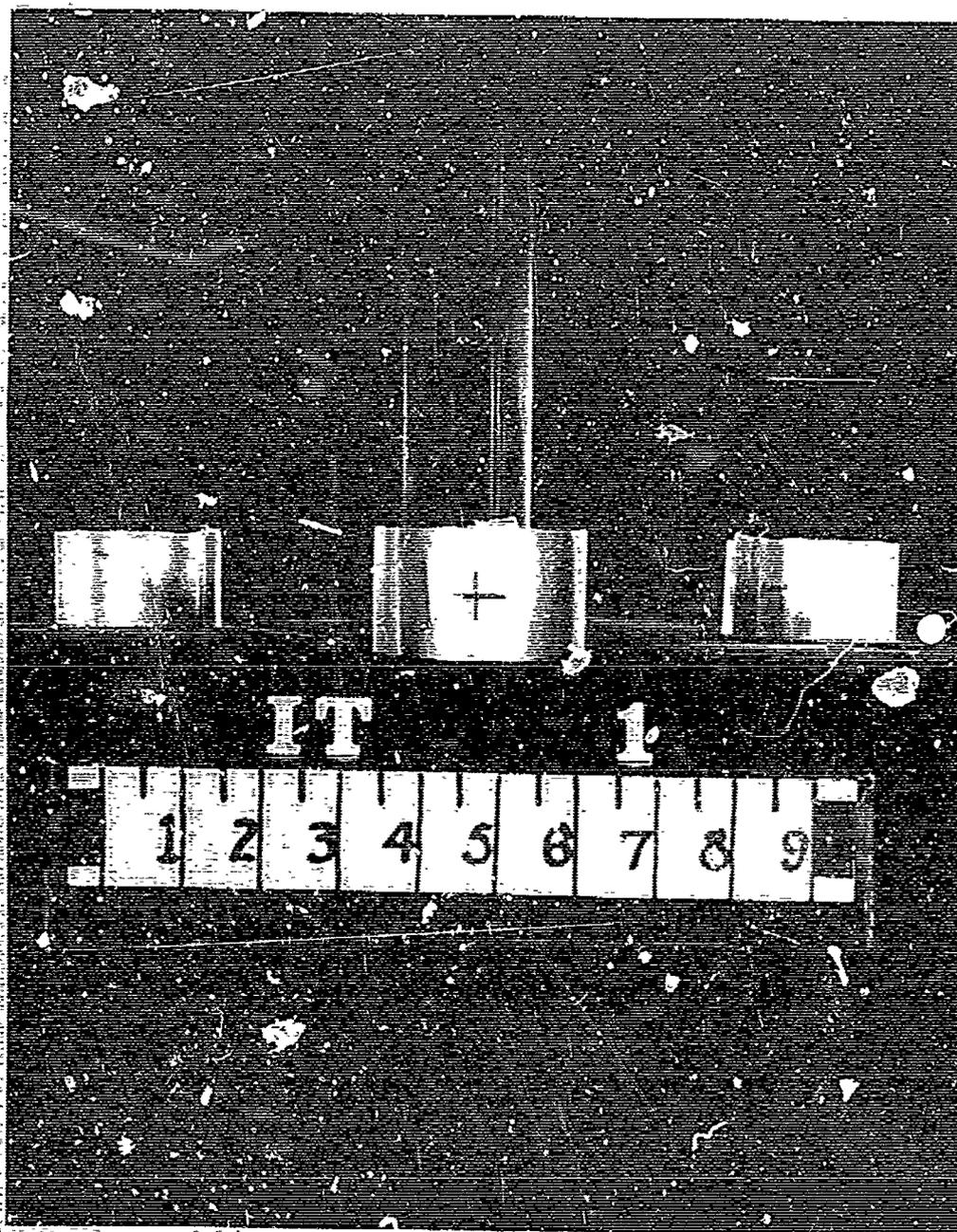
FIGURE D-3
Combination, 1100 - Al
D = 4.0 in., L/D = 3.4, D/h = 400

FIGURE D-4
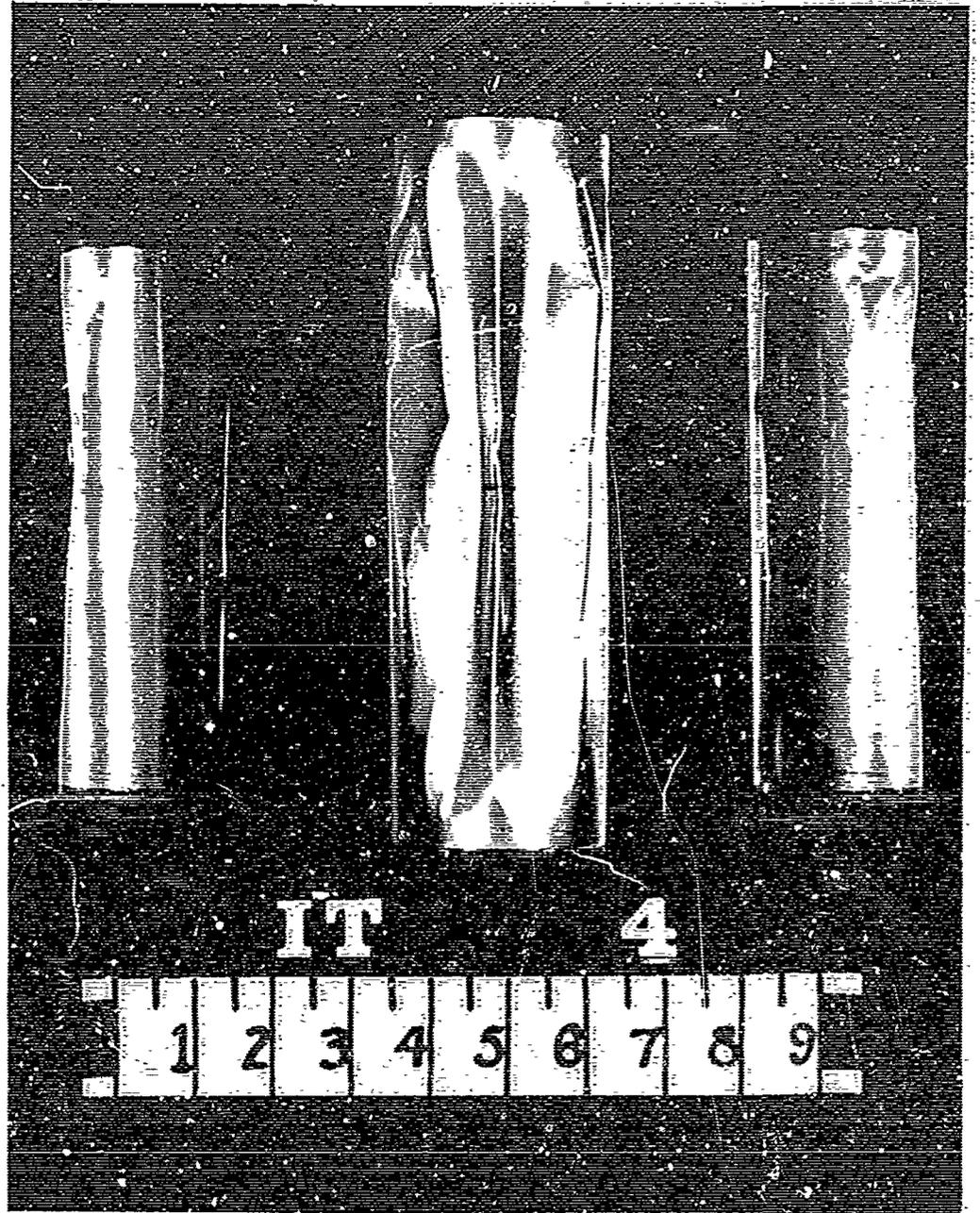Buckle, 5052 - Al
D = 3.0 inch, L/D = 0.33, D/h = 750

FIGURE D-5
Extensive Buckle, 5052 - Al
D = 3.0 in., L/D = 3.0, D/h = 1000

VITA

Richard Conrad Pees was born on 11 August 1945 in Pittsburgh, Pennsylvania. He graduated from Franklin Area High School in Murrysville, Pennsylvania, attended the University of Pittsburgh's Greensburg campus until January 1965 and then transferred to the main campus in Pittsburgh. While at the main campus, he was elected to Pi Tau Sigma National Mechanical Engineering Fraternity, Sigma Tau National Engineering Fraternity, Outstanding Sophmore in Engineering, and Co-Chairman of Engineer's Week 1967. He also was a member of the Arnold Air Society and Scabbard and Blade Military Honorary Society. He graduated in August 1967 Cum Laude and received his Bachelor of Science in Mechanical Engineering and a commission in the USAF. His first assignment was residence at AFIT - SE.

Permanent address: 4146 Old Wm Penn Hwy.
Murrysville, Pa. 15668

This thesis was typed by Mrs. Mary R. Pees.

DOCUMENT CONTROL DATA - R & D

Security classification of title, body of abstract and indexing annotation must be entered when the overall report is classified

1. ORIGINATING ACTIVITY (Corporate author)	2a. REPORT SECURITY CLASSIFICATION
Air Force Institute of Technology (AFIT-SE) Wright-Patterson AFB, Ohio 45433	Unclassified
	2b. GROUP

3. REPORT TITLE

Shell Parameter Influence on the Failure Mode of Side – On Air Blast Loaded Cylinders

4. DESCRIPTIVE NOTES (Type of report and inclusive dates)
AFIT Thesis

5. AUTHOR(S) (First name, middle initial, last name)

Richard C. Pees
2/Lt   USAF

6. REPORT DATE	7a. TOTAL NO. OF PAGES	7b. NO. OF REFS.
December 1968	102	15

8a. CONTRACT OR GRANT NO.	9a. ORIGINATOR'S REPORT NUMBER(S)
b. PROJECT NO.	
c. N/A	9b. OTHER REPORT NO(S) (Any other numbers that may be assigned this report)
d.	

10. DISTRIBUTION STATEMENT This document is subject to special export controls and each transmittal to foreign governments or forgeign nationals may be made only with prior approval of the Dean of Engineering, Air Force Institute of Technology (AFIT-SE) Wright-Patterson Air Force Base, Ohio 45433

11. SUPPLEMENTARY NOTES	12. SPONSORING MILITARY ACTIVITY

13. ABSTRACT

The purpose of this investigation is to determine the influence of the shell size parameters, length-to-diameter ratio and diameter-to-thickness ratio, on the failure mode of cylinders under side-on air blast loading. These failure modes are: (1) hinge collapse, (2) wave buckling, and (3) combination. The results of this study show that the diameter-to-thickness, (D/h), ratio dominates the shell behavior and that for values of D/h below 110, hinge collapse seems to be dominant; between 110 and 450, combination failure seems to be dominant; above 450, wave buckling seems to be dominant.

DD FORM 1473
1 NOV 63

KEY WORDS	LINK A		LINK B		LINK C	
	ROLE	WT	ROLE	WT	ROLE	WT
Shell Failure Modes						
Blast Loaded Cylinders						
Shell Influence on Failure Modes						